Forensic Science International 231 (2013) 375–396

Contents lists available at SciVerse ScienceDirect

Forensic Science International

journal homepage: www.elsevier.com/locate/forsciint

Review

Fluid dynamics topics in bloodstain pattern analysis: Comparative review and research opportunities

Daniel Attinger [a,*], Craig Moore [b], Adam Donaldson [c], Arian Jafari [a], Howard A. Stone [d]

[a] Department of Mechanical Engineering, Iowa State University of Science and Technology, Ames, IA 50011, USA
[b] Niagara Regional Police Service, St. Catharines, Ontario L2R 3C6, Canada
[c] Department of Process Engineering & Applied Science, Dalhousie University, Halifax, NS B3H 4R2, Canada
[d] Department of Mechanical and Aerospace Engineering, Princeton University, Princeton, NJ 08544, USA

ARTICLE INFO

Article history:
Received 9 November 2012
Received in revised form 2 April 2013
Accepted 17 April 2013
Available online 3 July 2013

Keywords:
Bloodstain pattern analysis
Review
Dimensionless number
Drop generation
Trajectory
Impact
Stain

ABSTRACT

This comparative review highlights the relationships between the disciplines of bloodstain pattern analysis (BPA) in forensics and that of fluid dynamics (FD) in the physical sciences. In both the BPA and FD communities, scientists study the motion and phase change of a liquid in contact with air, or with other liquids or solids. Five aspects of BPA related to FD are discussed: the physical forces driving the motion of blood as a fluid; the generation of the drops; their flight in the air; their impact on solid or liquid surfaces; and the production of stains. For each of these topics, the relevant literature from the BPA community and from the FD community is reviewed. Comments are provided on opportunities for joint BPA and FD research, and on the development of novel FD-based tools and methods for BPA. Also, the use of dimensionless numbers is proposed to inform BPA analyses.

Contents

* Corresponding author. Tel.: +1 515 294 1692.
E-mail address: Attinger@iastate.edu (D. Attinger).

0379-0738/$ – see front matter © 2013 Elsevier Ireland Ltd. All rights reserved.
http://dx.doi.org/10.1016/j.forsciint.2013.04.018

1. Introduction

While the disciplines of bloodstain pattern analysis (BPA) in forensics and that of fluid dynamics (FD) each have a rich history [1,2], interactions between these communities have not always been strong. From its infancy in 19th century Germany, BPA has aimed for practical answers to specific questions of the kind: "How did the bloodletting event of Fig. 1 happen?" FD was born in the 17th and 18th centuries, in England, Switzerland and France. In contrast to BPA, FD aims to quantitatively describe the motion of fluids (gases or liquids), and the causes of the motion, with general equations. FD typically defines the initial and boundary conditions of a fluid system, and from there describes how the system evolves in time and space, most often in a *deterministic* manner. BPA typically solves the indirect problem of inspecting stains in a crime scene to infer the *most probable* bloodletting event that produced these patterns. In both the BPA and FD communities, scientists study the motion and phase change of a liquid in contact with air, or with other liquids or solids. The need for better integrating FD and BPA is mentioned in a 2009 report [3] by the US National Research Council, entitled "Strengthening Forensic Science in the United States: A Path Forward". The report mentions that "the uncertainties associated with bloodstain pattern analysis are enormous", states that a minimum requirement to make BPA interpretations is to have "an understanding of the physics of fluid transfer", and advocates for stronger scientific foundations for BPA, given "the complex nature of fluid dynamics". It is our conviction that the FD and BPA communities could benefit from a deeper understanding of each other. Specifically, by following the path proposed by the US National Academies, BPA can obtain new quantitative tools and methods, while FD may be presented with new flow problems.

Note that there are two overlapping communities in BPA: the users and the researchers. BPA researchers, the specific target of this review, evaluate existing BPA techniques, for example for accuracy; they also develop new BPA techniques. Their research is typically funded by Governmental Agencies, run in Government laboratories or in universities and published in journals such as Forensic Science International or the Journal of Forensic Sciences of the AAFS (American Academy of Forensic Sciences).Users of BPA techniques study specific crime scenes, funded by the Police Administration or when hired as trial consultants. Articles with direct practical relevance, targeting users, are typically published by the International Association for Bloodstain Pattern Analysis (IABPA) Journal or the Journal of Forensic Identification of the International Association for Identification (IAI). A better integration of FD and BPA might provide better, or simpler tools for BPA users. Also, some of the ideas in the manuscript may be useful to instructors for either identifying science topics useful for education of future practitioners or for contributing to the continual education of practitioners interested in introducing more scientific approaches into their work.

This review is organized in five parts. First, Section 2 describes the *physical forces* driving the dynamics – the motion and its causes - of blood as a fluid. Then, the formation of bloodstains is described as a deterministic sequence of events, in separate sections on *(3) drop generation, (4) drop trajectories, (5) drop impact, and (6) stain formation*.

For each of the five topics listed above, a summary and comparative review of relevant literature is presented, first the BPA literature, and then the FD literature. The purpose of this manuscript is to describe the FD themes and research topics that affect BPA. It is not intended to be a review of each individual field, but a comparative review of the overlapping areas to facilitate identification of potential inter-community collaborations. For instance, a synthesis of the connections between FD and BPA is proposed in Section 7, describing how well the problems are understood and what opportunities exist for new research and the development of novel tools and methods. The findings of our review paper are then summarized in Table 4, which highlights the relations between BPA terminology (rows of the table) and FD concepts (columns). It is our hope that this manuscript will be used to assess the state-of-the-art and to identify untapped research topics at the intersections of FD and BPA.

Fig. 1. BPA uses FD-based methods to reconstruct a bloodletting event. In the above crime scene investigated by one of the co-authors, C.M., various bloodstain patterns are visible, namely a pool (AE), transfer stains (AB), flow patterns (AA) and several drip stains (AD). Elliptical bloodstains (B) indicate the area of origin of a blood spatter, see Section 5. For an interpretation of what happened in the photographed crime scene, refer to Section 8.

Table 1
Physical properties and parameters relevant to the FD of BPA, with controlling factors. Typical values are given, while the intervals in parenthesis correspond to the published range of value.

Liquid properties	Human blood	Animal blood (species dependent)	Distilled water	Sources, Control Factors and Notes
Viscosity, μ ($\times 10^{-3}$ kg/ms)	20 °C: 6.3 37 °C: 4.4 (1.6 – 5.1)	20 °C: 8.6 37 °C: 5.5 (3 – 20)	20 °C: 1.0 37 °C: 0.7	[1,4,7,15–18] *Temperature, shear rate, hematocrit*
Surface tension between air and liquid, σ ($\times 10^{-2}$ N/m)	20 °C: 6.1 37 °C: 5.2 (2.7 – 5.8)	20 °C: 6.5 37 °C: 5.1	37 °C: 7.0 20 °C:7.3	[1,4,7,19,20] *Temperature, shear rate, hematocrit*
Density, ρ (kg/m^3)	1060 (1052 – 1063)	1062	993	[4,19] Values at 37 °C
Hematocrit, H	0.40 (0.40 – 0.45)	0.4 (0.39 – 0.46)	0	[1,4,19]

Target properties	Range of values	Control factors and notes
Surface roughness, Ra (m)	1×10^{-10}–1×10^{-2}	Material, manufacturing process and surface preparation
Wetting angle, θ (degrees)	0 (very clean glass) – 140 (waxed car)	Material, manufacturing process and surface chemistry
Elasticity, E ($\times 10^9$ Pa)	0.001 (rubber)–1000(diamond)	Material
Permeability, k (m^2)	1×10^{-7} (gravel)–1×10^{-19} (granite)	Material and internal microstructure, can be predicted with the Kozeny–Carman model. [21]
Porosity, ϕ (m^3 void/m^3 material)	0–0.4	Material and internal microstructure

Impact and drying scales	Range of values	Control factors and notes
Velocity, v (m/s)	0–100	Low velocities typical of free-falling droplets; high velocities typical of gunshot scenarios–
Diameter, d ($\times 10^{-3}$ m)	1×10^{-3} (1 μm)–5 (5 mm)	Smaller drops are typically released in high-energy, high-velocity situations–
Shear rate, γ (1/s)	0–20,000	The larger shear rate corresponds to the impact at 100 m/s of a 5 mm drop on a target–
Volume, V ($\times 10^{-9}$ m^3)	5.2×10^{-10} (0.5 fL)–65 (65 μL)	Volume of a blood drop
Mass, m ($\times 10^{-6}$ kg)	6×10^{-10} (0.6 pg)–69 (69 mg)	Mass of a blood drop

2. Physical forces at play in bloodstain pattern analysis (BPA)

2.1. Description in the BPA literature

Several classic BPA textbooks [1,4,5] include a comprehensive section on the biological and physical properties of blood, describing this complex fluid and its main physical properties, such as density, viscosity and surface tension. Typical values of these properties are provided in Table 1. Generally defined, blood is an aqueous liquid, with about half of its volume consisting of micrometer-size particles such as red and white blood cells. An indicator of the concentration of particles in the blood is the hematocrit, which is the measurement of the relative volume of red blood cells versus the total blood volume [1]. The density of blood, its mass per volume, 1060 kg/m^3, is close to that of water. The same textbooks also describe how the porosity, roughness and wettability of a blood-stained surface, called the target surface, influence the observed stains. Viscosity is typically presented as a measure of the resistance of a fluid to a change of shape or flow [5]. The viscosity of blood at body temperature is reported as approximately four times larger than that of water [5]; the viscosity of blood decreases with increasing temperature [5] and increases with increasing hematocrit [6]. Blood is also described as non-Newtonian fluid, i.e. a fluid with a viscosity that varies with the flow conditions [5].

Surface tension, also referred to as the surface energy, is the measure of the energy to change the interfacial area between two immiscible fluids, here blood and air. Surface tension plays a key role in the generation of drops and their impact on surfaces. Surface tension decreases with increasing temperature and is affected by chemicals present within the blood [7].

Often, BPA work reports measurements of velocities, drop sizes or stain sizes corresponding to a specific experiment [8,9], without attempt to generalize the conclusions to other experimental conditions. Sometimes empirical correlations are fitted to a set of BPA data [10–12] with little consideration for the physical basis of these correlations or for their domain of validity. These approaches might induce conceptual errors and possibly could be replaced by a physical and dimensionless description, as in [13,14], to compare the relative importance of the physical forces. These ideas are discussed in more details below.

Table 2
Forces and typical dimensionless parameters used to describe FD phenomena, with typical magnitudes in BPA cases.

Force	Physical expression	Magnitude in BPA, in N (Newton)	Physical meaning
Inertial force	$\rho v^2 d^2$	0 to 265	Mass × maximum possible acceleration of a moving volume of fluid, i.e. a drop
Capillary force	$\sigma d \cos\theta$	−4 to 5	Force due to surface tension, parallel to the interface between two fluids, acting on the 3-phase line (see Fig. 2)
Viscous force	$\mu v d$	0 to 2×10^{-3}	Dissipative forces due to friction in a moving fluid
Gravity force	$\rho g d^3$	0 to 0.001	Attractive force acting on a volume of fluid, directed towards the center of the earth

Dimensionless number	Definition	Magnitude in BPA	Ratio of forces
Reynolds number	$Re = \rho v d/\mu$	0 to 100,000	Inertia to viscous forces, describes the drag during the flight of a drop and the impact of a drop on a surface
Weber number	$We = \rho v^2 d/\sigma$	0 to 1×10^7	Inertia to surface tension forces, describes jetting, impact and drop oscillations
Capillary number	$Ca = \mu v/\sigma$	0–8	Viscous to surface tension forces, describes wetting and imbibition
Bond number	$Bo = \rho d^2 g/\sigma$	0–5	Gravity to surface tension forces, controls spreading of large drops or streams; establishes the shapes of static drops
Froude number	$Fr = v^2/dg$	0 to 1×10^{12}	Inertia to gravity, controls spreading and flight of drops
Drag coefficient	$C_D = F_D/\frac{1}{2}\rho_a v^2 A_d$	0.3 to 1×10^5	Ratio of the drag force to the stagnation pressure force caused by the motion of the drop in air

2.2. Fluid dynamics description

In FD, a fluid is characterized in contrast to a solid, and with respect to some physical properties. What defines a liquid versus a solid is the deformation in response to stresses like shear or elongation: solids respond to stresses by a sudden deformation, until a new equilibrium configuration is reached, while fluids continually deform as long as a shear stress is applied. Within FD, the viscosity is defined as the ratio between applied stress and the rate of fluid deformation: the higher the viscosity, the higher the stresses needed for the same fluid deformation (or flow). Viscosity dissipates the energy associated with the deformation of a fluid. In relation to BPA, viscosity dampens the shape oscillations of drops in flight and resists the spreading during impact. The viscosity of liquids typically decreases with increasing temperature.

For complex liquids such as blood, which contain suspended particles, the viscosity changes with the shear rate (see Table 1 for values of shear rates representative of BPA). Such a fluid with a non-constant relation between stress and rate of deformation is called *non-Newtonian*. Blood is further classified as shear-thinning, a specific class of non-Newtonian fluids for which viscosity decreases with increased shear. Indeed, blood appears more viscous when it drips from a wound than when it impacts a target at several meter/second. The viscosity of the blood also increases with increasing hematocrit and decreasing temperature. The viscosity μ of blood can be modeled from experiments in the form [16] of $\mu = \mu_{ref} g(H) f(\gamma) k(T)$, where μ_{ref} is the viscosity at a reference level of temperature (typically 37 °C); and the respective functions g, f and k model the dependence on hematocrit, shear rate and temperature, respectively. Other models do exist, such as that given in [22], to describe the measured viscosity of human blood for shear rates from 2/s to 100,000/s.

Surface tension is a force over a length, or an energy per unit area, that characterize any interface between two materials of different physico-chemical structure, such as blood and air. Surface tension affects the drop formation process, the breakup of jets [23] and the oscillations of the shapes of drops. Surface tension tends to keep the drops spherical in flight since spherical shapes minimize the surface energy [24]. This tendency of drops to assume a spherical shape is important to BPA, especially in relation with the determination of impact angles from the ellipticity of stains.

Regarding the target substrate, the important physical properties are the elasticity, permeability, porosity, roughness and wetting angle. The elasticity E of a target is the ratio of the applied normal force per area to the resulting relative deformation of the solid surface, called the strain. For example, microscopic deformations of a rubber target during drop impact have been shown to influence the splashing of the drop [25]. The permeability is related to the ability of a liquid to flow through a porous target. The porosity is a measure of the typical pore space available for a fluid [21]. The roughness is a representative measurement of the departure of the surface texture from an absolute flatness; it is commonly expressed as *Ra*, the arithmetic average of that departure. The wettability describes how a solid target influences the motion of a pair of immiscible fluids along it [26], for example water/air or water/oil. In BPA, wettability influences the stain size and their drying. In the case of BPA, the system of interest involves the two fluids of blood and air, as well as a solid target. The wettability of a system is illustrated in Fig. 2, and depends on the system chemistry, physical state (cold or hot) and target microstructure or roughness. It is characterized by the wetting angle measured at the edge (also called the wetting or contact line) of a small drop on top of the target, referred to as the static wetting angle. A small wetting angle ($\theta \sim 0^\circ$) corresponds to a hydrophilic state, while a large wetting angle ($\theta > 120^\circ$) correspond to a hydrophobic state, as the liquid tends to be repelled from the substrate. Note that the wetting angle dynamically adjusts its value when the wetting line moves, for example during impact or evaporation [27].

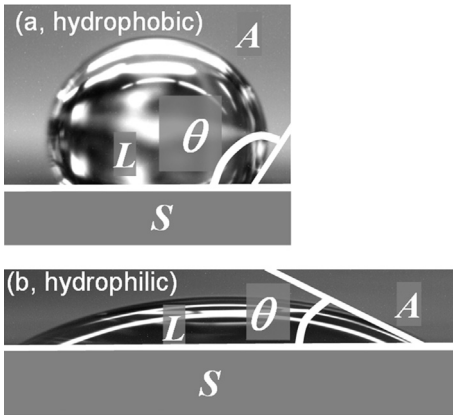

Fig. 2. Wetting angle θ on a hydrophobic target (*a*, such as an oily, plastic or waxed surface) and on a hydrophilic target (b, such as clean glass). The wetting angle is measured at the three-phase line, which is the location where the air (A), the liquid (L) and the solid (S) meet. Drop impact and stain formation depend on wettability.

Dimensionless numbers

The discipline of FD describes the motion of gases in extra-terrestrial space [28], the dynamics of atmospheres and oceans, and the motion of blood in capillaries thinner than a human hair [29]. To describe within a single framework events that span such a large range of time and length scales, FD relies on a three-step analysis: first, the magnitude of all the forces acting on the fluid are evaluated, as in Table 2; then the relative magnitude of pairs of these forces is compared using scaling or dimensionless numbers, such as the ones listed in Table 2, for example the Reynolds or Weber number; finally a more detailed analysis is performed based only on the most relevant forces, neglecting those that are comparatively negligible. FD methods for detailed analysis include various analytical methods (solving FD equations with pen and paper), numerical methods (solving FD equations with a computer), or experimental methods (for example high-speed visualization). On one hand, detailed FD analyses provide accurate solutions, but can be cumbersome and mathematically challenging. On the other hand, proper use of dimensionless numbers result in simpler analyses valid for a wide range of experimental conditions, allowing experimental outcomes (stain dimension, number of spines, splashing versus no splashing) to be inferred for cases that have not been (*or can not be*) tested explicitly. In other words, the fluid dynamicist knows that two liquids behave similarly as long as they are in the same physical regime, i.e. as long as they are experiencing the same ratios of forces. Therefore, what influences BPA events is not so much the physical properties of the blood, air and target, or the velocities of the bloodletting event, but rather the balance between the forces at play, expressed with dimensionless numbers. Indeed, these Reynolds and Weber numbers are not a way to express practical data (such as velocities or length) in a more complicated way, but they help answer practical questions. Sections a-c below illustrate the importance of dimensionless numbers with the elementary BPA problem of determining the impact velocity v of a drop with diameter d moving downwards towards a target.

(a) A dimensionless curve replaces multiple dimensional curves: Let us start with the simplest experiments where a drop from a dropper drips towards the ground. Let us control the height h of the fall and measure the duration t of the fall with a chronometer or with a high-speed camera. Like Galileo [30,31], we find, at least for moderate heights, that h is proportional to t^2,

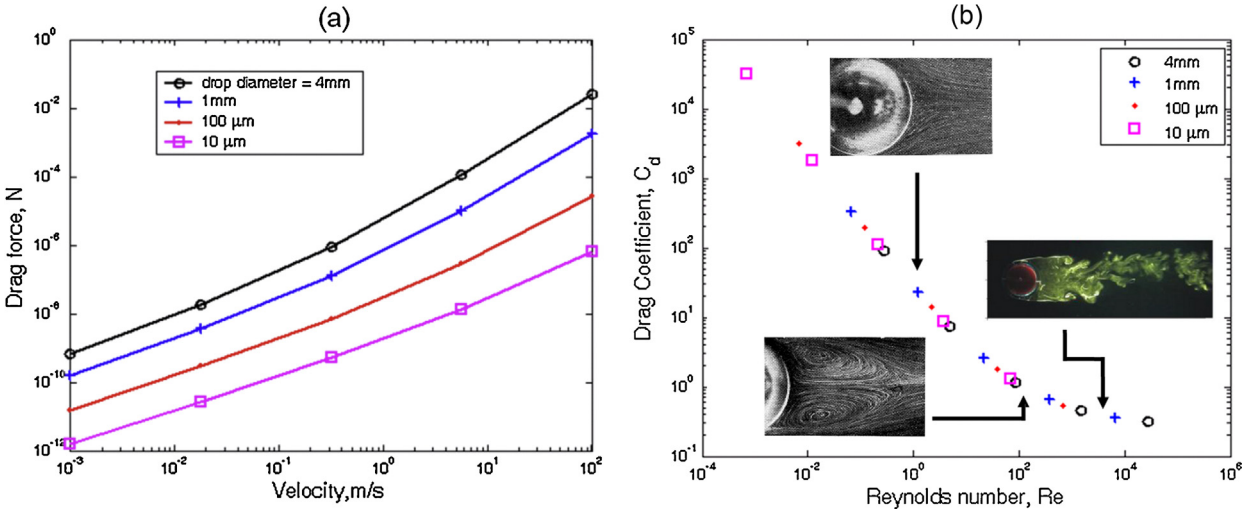

Fig. 3. Determination of the drag force as a function of the velocity of a spherical drop moving through quiet air. Dimensional plot (a) versus non-dimensional plot (b). Note that in (b) all the datapoints collapse onto the single line of Eq. (3) when reported using dimensionless numbers. In the photographs, the general fluid flow direction around the sphere is from right to left, seen with particles added to the fluid. Photographs reprinted from [32], Copyright (1956), with permission from The Physical Society of Japan; and from [33], Copyright (2011), with permission from Elsevier.

i.e. $h \cong t^2$. Using together the measured values of h (in meter, noted m) and t (in second, noted s), and the physical principle that a valid equation needs to have the same units on both sides of the equal sign, we find the equation for the travel of the drop as $h = 1/2gt^2$, where we have identified in g the gravity constant with units of, necessarily, m/s^2. We might then realize that a drop that falls from higher than one meter typically takes more time than predicted by the equation $h = 1/2gt^2$. The culprit for slowing down the drop is the drag, the resistance force exerted by the air on the moving drop. Fig. 3a shows values of the drag force on spherical drops moving through air, as a function of their velocities and diameters. The drops have various diameters, representative of BPA situations. For low velocities and small drops, the relation is a straight line because the drag force is proportional to v; for larger and faster drops, the relation becomes a parabolic curve indicating that drag forces become proportional to v^2. The transition between these two behaviors (proportional to v and then to v^2) occurs at different velocities for different droplet sizes.

In contrast, Fig. 3b describes the same relationship between drag and velocity in a dimensionless way, and all the results of Fig. 3a collapse along a single curve. To do so, the drag force is reported as the drag coefficient (C_D, defined as in Eq. (2) and (3) below) and plotted against the Reynolds number (defined in Table 2). The information conveyed with the dimensionless plot in Fig. 3b is the very same as in the dimensional plot of Fig. 3a, except that one dimensionless curve replaces several dimensional curves.

(b) A dimensionless plot tells more about the physics at play than multiple dimensional plots: In the dimensionless plot of Fig. 3, the transition between a linear and parabolic relationship between the drag coefficient and the velocity v corresponds to the transition between the region where C_D decreases with Re, and the region where C_D is constant with Re. This transition occurs over a well determined range of Reynolds number, corresponding to a change of physical regime, i.e. a change in the respective importance of inertial and viscous forces (Table 2): at low Re the flow is steady and drag is mostly caused by friction forces, corresponding to a linear dependence between C_D and Re, while at Re higher than ~100 unsteadiness and turbulence develop, as exemplified by the pictures of the flow at $Re > 10^4$. This chaotic motion of the air around the droplet corresponds to inertial forces being the main cause of the drag, overcoming viscous forces, and results in a parabolic relationship between C_D and Re. *The ability to see the transitions between dominant forces comes with the use of dimensionless numbers in FD.*

An illustrative example of the advantages *a* and *b* of using dimensionless numbers in BPA is provided by the impact velocity map elaborated in Fig. 4. This map provides the impact velocity (expressed by the contours of ratios of impact velocity to terminal velocity) of a drop striking a target, as a function of the initial release conditions (i.e. initial drop diameter d_0 and initial velocity v_0). For simplicity in Fig. 4, v_0 is oriented downwards, and the target is placed horizontally, one meter below the release location. The initial conditions in Fig. 4 are representative of various conditions encountered in BPA, with 10^{-3} mm $\leq d_0 \leq$ 5 mm and 0.1 m/s $\leq v_0 \leq$ 240 m/s.

In this situation of a drop flying towards a target, only two forces are active: the weight of the drop, and the drag between the drop and surrounding air. The motion of the droplet towards its target can be accurately computed, considering how these two forces affect its initial velocity and position during the flight. Mathematically, this motion is described by Newton's second law:

$$m_d \frac{d\vec{v}}{dt} = m_d\vec{g} - \vec{F}_D, \tag{1}$$

where $m_d, d\vec{v}/dt, \vec{g}$ and $\vec{F}_D$ are the droplet mass, droplet acceleration, gravitational acceleration and drag force, respectively. The above equation simply means that during the time of its flight, the velocity of the droplet is modified by two forces, its weight and the drag.

The value of the drag force is expressed with the correlation

$$\vec{F}_D = \rho_a C_D \frac{A_d}{2} \vec{v} v, \tag{2}$$

where ρ_a, A_d, v and $\vec{v}$ are the air density, the cross-sectional area of the droplet, the velocity magnitude and velocity vector of the droplet. The dimensionless parameter C_D is the drag coefficient of a spherical object such as a drop, as plotted in Fig. 3b. For BPA cases, C_D is best expressed by the correlation of Lavernia et al. [34]:

$$C_D = 0.28 + \frac{6}{Re^{0.5}} + \frac{21}{Re}, \quad \text{valid for } 0.1 \leq Re \leq 4000. \tag{3}$$

Fig. 3b shows how C_D varies with the Reynolds number $Re = \rho_a v d/\mu_a$, where ρ_a, μ_a, v and d are the density and dynamic viscosity of the air, and the droplet velocity and diameter,

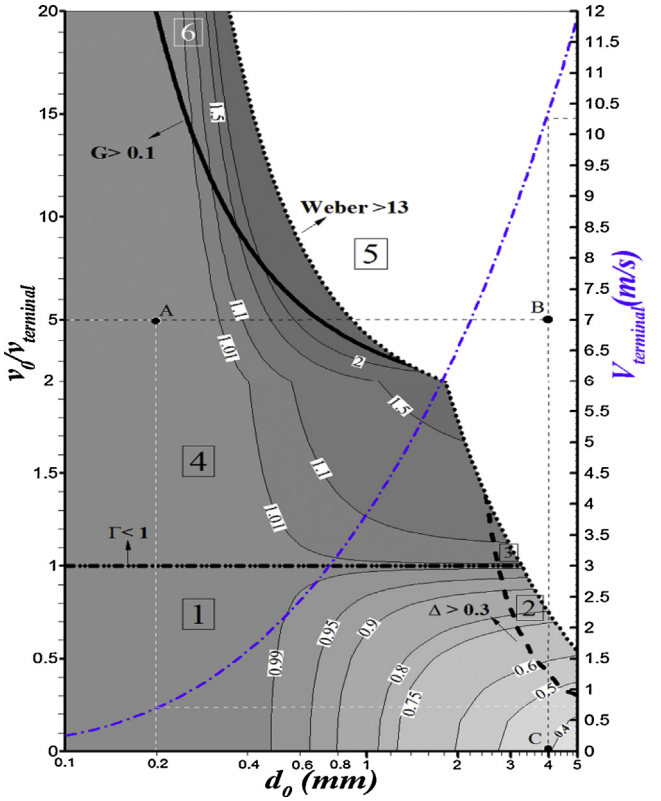

Fig. 4. Semi-dimensionless plot to determine the impact velocity of a falling droplet as a function of droplet diameter, d_0, and initial droplet velocity, v_0, for a vertical path (trajectory) of 1 m. The initial velocity points downwards. Note that both axes are non-linear to better display the data. Both the impact velocity (thin contours in the body of the plot) and the initial velocity are given in a non-dimensional manner, as ratios over the terminal velocity. The terminal velocity $v_{terminal}$ is the dash-dot violet curve, with values on the vertical axis, right. The thick lines delineate various physical regimes, identified with squared numerals and described in Table 3 and point 2.2b. Detailed instructions to use the plot are in Appendix B.

respectively. The impact velocities and terminal velocities in Fig. 4 have been integrated with respect to time using Eq. (1), with an explicit discretization method that was tested for convergence.

In a plot such as Fig. 4, non-dimensional numbers are used in many ways: first the initial velocities (vertical axis) and impact velocities (contours) are displayed as ratios relative to the terminal velocity. This allows the presentation of a wide range of velocities in the same plot, more accurately than if velocities were plotted dimensionally. Also, the different physical regimes are best identified with dimensionless numbers and correspond to specific regions indicated by squared numerals in Fig. 4. Let us show now how these different physical regimes are related to the following questions, fundamental for BPA studies.

b1. Will the drop break into smaller drops? In flight, breakup occurs when the aerodynamic force, i.e. the drag of the air on the droplet, overcomes the surface forces at the droplet-air interface. In-flight breakup complicates the reconstruction of trajectories. The larger the drop and the higher the velocity, the higher the chances that the drop breaks up during its flight. To evaluate the possibility of breakup more rigorously, the aerodynamic drag force is compared with the surface force [35]. This comparison is expressed with the dimensionless Weber number,

$$We = \frac{\rho_a v^2 d}{\sigma}, \tag{4}$$

where ρ_a, v, d, and σ are the density of air, maximum velocity, droplet diameter, and surface tension, respectively. Should *We* be significantly smaller than *1*, the droplet travels without breaking up, because surface tension forces win over drag forces. Should *We* be on the order of *1*, the droplet will significantly deform. At even larger *We*, the deformation becomes so severe that the drop disintegrates into smaller ones, when drag forces overcome surface forces. While the reasoning above is based on a dimensionless FD number, experiments are needed to determine the exact value of the Weber number above which drop breaks up. As shown in [36,37], breakup typically occurs for $We > 13$, i.e. in the region above the thick dotted line in Fig. 4, plotted for values of $We = 13$ based on the initial drop diameter and velocity. As a result, no impact velocities are provided above that line, because the formalism exposed here cannot predict how in-flight break-up affects the trajectory.

Table 3
Significance of the physical regimes, shown as specific regions in Fig. 4.

Physical Regime	Physical significance on the trajectory of a drop
1	Significant acceleration of droplet due to gravity forces, drag forces are significant
2	Significant acceleration of droplet due to gravity, drag forces are insignificant
3	Minor deceleration of droplet due to drag, gravity negligible with respect to drag, but gravity significant with respect to initial kinetic energy
4	Drag forces significantly decelerate the drop; gravity negligible with respect to drag, but gravity significant with respect to initial kinetic energy
5	High probability that drop breaks up into smaller drops during flight, due to shear breakup
6	Major deceleration due to drag; gravity negligible with respect to initial kinetic energy

b2. Will gravity forces significantly modify the initial velocity?

The question of the influence of the gravitational force on the trajectories is important in BPA. If acceleration due to gravity is negligible during the droplet's flight, there is no need to consider curved trajectories. Gravity forces act all along the trajectory, but do they significantly modify the trajectory? For the specific case in Fig. 4, gravity will significantly modify the initial velocity if the work of the gravity along the droplet path, W_g, is significant with respect to the initial kinetic energy of the drop E_{k0}. This comparison is expressed as the dimensionless number

$$G = \frac{W_g}{E_{k0}}, \tag{5}$$

and shown in Fig. 4, where a thick solid line delineates the region $G > 0.1$. To the left of that line, gravity forces will modify the initial velocity significantly, while to the right of that line, gravity forces will not modify significantly the initial velocity. An exact expression of G is given in Appendix A.

b3. Will the drag force significantly affect the trajectory?

The question of the influence of the drag force on the trajectories is important in BPA. If drag is negligible, then ballistic trajectories can be calculated without accounting for the drag force –which is a complicated function of the drop velocity, see Eq. (3).

In layman's terms, the question of interest is "Will the drag forces slow down the drop a lot or just a little bit?" To answer that question in FD terms, the work W_D of the drag forces along the entire trajectory needs to be compared with the initial kinetic energy of the drop, E_{k0}.

This comparison is expressed by the dimensionless number

$$\Delta = W_D / E_{k0} \tag{6}$$

Should Δ be significant, then the work of drag forces will modify the initial velocity significantly. Should Δ be negligible, then the drag forces will not modify significantly the initial velocity

along the trajectory. For example, if a cloud of drops is produced with a given velocity, the larger drops typically travel further away from the region of origin, because their Δ value is smaller than that of the smaller drops. This phenomenon explains why for example in gunshot spatters the small stains are found closer to the area of origin.

Due to the change in velocity along the droplet's path, both W_D and Δ need to be calculated numerically (with a computer, according to the full definition of Δ in Appendix A). In Fig. 4, a thick dashed line delineates the region where $\Delta > 0.3$. The region left from this curve corresponds to a significant slowing down of the initial drop velocity by the work of the drag forces, while the region right from the curve correspond to a negligible effect of the drag forces on the initial drop velocity. Note that the terminal velocity of a droplet is the velocity at which drag forces and gravity forces are in balance (the dash-dot violet dash-dot curve in Fig. 4).

b4. Will the drop accelerate or slow down?

This question is best answered by comparing the respective magnitude of the gravity force and the drag force. This ratio is expressed with the dimensionless number

$$\Gamma = mg/F_D \tag{7}$$

In the above expression, the drag force can be analytically calculated based on the initial velocity from Eq. (2). In Fig. 4, the black dash dotted line delineates the limit where $\Gamma \leq 1$; above that line drag forces dominate and the drop slows down; below, gravity dominates and the drop accelerates. The terminal velocity of a droplet corresponds to the situation where gravity and drag forces are in exact balance. It is a function of the droplet diameter and is indicated by the dash-dot violet curve in Fig. 4.

As a summary, Table 3 lists the following six physical regimes corresponding to specific regions in Fig. 4. While Fig. 4 has been drafted for the pedagogical purpose of showing the use of dimensionless numbers, similar regime maps might help discriminating situations where gravity and drag forces matter, from situations where these do not matter. This might be relevant to the selection of methods to reconstruct the trajectories of blood drops.

(c) Dimensionless numbers are useful for designing experiments. For instance a large blood drop impacting a target at low velocity might behave in a similar way as a smaller drop impacting a target at higher velocity. *While the latter experiment might be very hard to make, the former might be easier to make.* The fundamental reason behind this is that two physical events will behave in a similar way if the ratios of physical forces are the same, i.e. if the values of the relevant dimensionless numbers (here, the Reynolds number as well as other relevant numbers) are matched, see point (b) above. For more details on the use of dimensionless numbers, see the discussion on similarity and dimensional analysis by Sedov and Barenblatt [38,39].

As a summary, the use of dimensionless numbers helps to

(a) replace multiple dimensional plots by a single dimensionless plot;
(b) determine what physical forces influence a specific phenomenon (here the impact velocity of a drop), and what physical forces can be neglected; and
(c) design experiments.

3. Drop generation

3.1. Description in the BPA literature

BPA analysts often describe single stains or *spatters* (group of stains) with a terminology that indicates the most probable mechanism of their generation [5]. These terms, with several other commonly used in BPA, are defined in Table 4a. The terminology is based mainly on the recognition of typical spatters, in terms of their spatial distribution, the size distribution and orientation of their stains (for example converging radially or aligned). Indeed, a beating causes several individual and clearly visible mm-stains, while a shooting causes a preponderance of sub-mm overlapping stains, a pink layering called "pinking" or atomized mist. For example, the terms *drip stain* refer to drops that fall when their weight overcomes capillary forces, while *cast-off patterns* refer to spatters of drops generated when acceleration forces overcome capillary forces. Other spatter terminology hinting at the generation mechanism include *impact pattern*, *mist pattern*, *back spatter pattern, forward spatter pattern, pool*, *swipe pattern*, *splash pattern*, *bubble ring*, *projected pattern* and *expiration pattern*. These spatters of known origin are routinely generated and studied in the workshops educating the BPA examiners.

Two assumptions have been used in BPA studies to correlate the size distribution of stains in the spatter to the mechanism that generated the spatter:

1) the stain size correlates inversely with the momentum or speed of the generation event [4];
2) the stain size indicates the drop size (see discussion in Section 5.1.2). For instance, [43] mentions that "The mass of the blood drop can be estimated approximately by the diameter (width of the bloodstain) and the density of blood."

The direct observation of the dynamic generation of a blood spatter is challenging, because of the high speeds involved (a baseball bat swings at more than 30 meter/second [44]) and the sizes of the objects to monitor (sub-mm drops are produced in a gunshot spatter). Early attempts of high-speed visualizations in BPA have been reported in 1939 [42], when the oblique impact of mm-size drops was recorded with an analog camera at speeds up to 250 images/second. The report [42] mentions two difficulties: the need for lot of lighting, and the difficult synchronization between the recording and the event. The more recent video "Blood in Slow Motion" [45] shows recording at 4000 images per second. The sequences show the formation of blood drops, normal and oblique impacts on solid surfaces of various roughnesses and porosities, impacts on liquid blood pools, and the formation of castoff spatters. With the advent of digital high-speed cameras in the late 1990s, the issue of synchronization has been mitigated, and speeds up to 1 million frames per second have been made possible. For instance, strobe photography and high-speed camera visualization have been used in BPA for expirated [46] and gunshot spatters [47,48]. In the latter case, information was gathered on the complex interaction between the air flow induced by the gunshot and the flight of the cloud of sub-mm droplets. The best examples of digital high-speed videos related to BPA are the extensive studies [48,49] done by Epstein, Laber and Taylor. The related publicly available dataset [50], which is the source of Figs. 6 and 10, has brought attention in the BPA community to the complexity of the associated fluid dynamics phenomena.

3.2. Fluid dynamics description

Fluid dynamicists have a long tradition in studying the generation and impact of drops for the purpose of technologies such as fuel atomization, ink-jet printing, additive manufacturing, painting, agriculture, or for the intellectual pleasure of understanding how nature works. These studies involve sketches by *da Vinci* [51], Savart [52] and Worthington [53], see Fig. 5A and B. Drawings by Worthington are the first examples of high-speed visualization of drop impact, and a remarkable testimony of

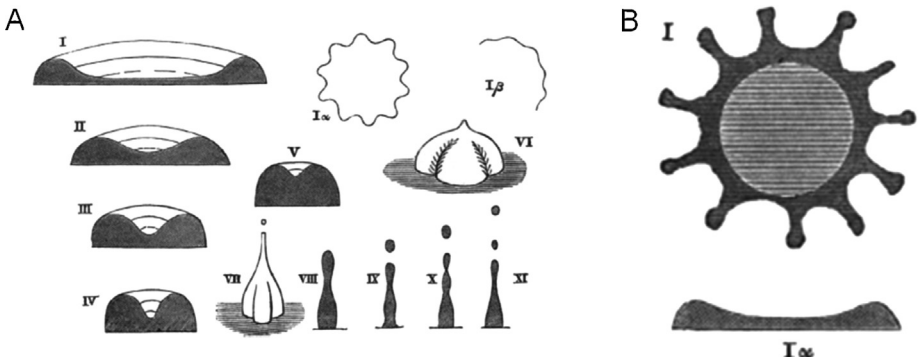

Fig. 5. Early attempts of visualizing drop impact. (A-B) show various shapes assumed by a drop of milk impacting on a glass target, as sketched in 1876 by Worthington, without a camera, but with the help of an electrical spark generator and of his retinal persistence. Hand-drawn sketches show ring accumulation during the impact, splashing and the formation of spines. Reproduced freely from [54], the content of which being out of copyright according to the Royal Society.

mankind's creativity. In the late 1800s, Worthington used short and intense electric sparks to impress his retina and 'freeze' the motion of impacting water and mercury drops. Patching together several of these sketches taken at different instants of the impact, he could sketch without camera a sequence of drawings of drops deforming during impact, achieving a time resolution better than a millisecond [53,54]. Current commercially available high-speed cameras can conveniently record continuous movies from events at frame rates up to 100,000 frames per second [55]. Using similar principles as Worthington, but faster flashes and sensitive cameras, FD phenomena have been imaged in research laboratories at frame rates up to one million frames per second [56]. Femtosecond lasers provide even faster illumination, and frame rates up to one *trillion* frames per second are even possible [57], as long as the investigated phenomena are reproducible at these timescales.

Several other non-intrusive experimental technologies are applicable to measure the dynamics of drop generation, flight and impact, in terms of particle size, velocities, temperatures, composition and their distributions, as reviewed in [58–60]. The technologies include particle image velocimetry, laser-induced fluorescence and laser-Doppler methods.

The dynamics of drop generation is also well documented for the following processes: dripping, sheet breakup and jet breakup.

Dripping occurs when a slowly growing volume of liquid suspended by capillary forces is detached as a drop by gravity forces. Inertial and viscous forces typically play a secondary role because the process is slow. The debate [40,41] in the BPA community about the existence of a typical or minimum volume of a blood drop generated by dripping can be resolved as follows: this volume depends on the balance between gravity and the vertical projection of the capillary force, rather than simply on the balance between gravity and surface tension. While surface tension only depends on the solid and the fluids in contact, the vertical projection of the capillary force depends also on the wetted diameter and wetting angle (see Table 2), i.e. on the shape and material of the object from which the drop drips. Therefore, dripping drops with a wide range of volumes can be generated by changing, for example, the diameter or material of a pipette, as already mentioned in the French version of the early BPA work of Balthazard et al. [42].

The dripping phenomenon is well understood [61,62] in terms of kinematics [63], frequency, drop volume and "pinch-off length", which is the distance where a drop separates itself from its source. Viscosity influences the dripping process of Newtonian [64] and non-Newtonian fluids [65]. If the flow rate that causes the initial volume of liquid becomes faster, inertial forces come into play (as indicated by non-negligible Weber numbers). Inertial effects affect the drop size, the formation of smaller "satellite" drops [66]. At even faster flow rates dripping transitions towards jetting, when the Weber number reaches a critical value [67]. Also, dripping and jet breakup induce longitudinal oscillations in the generated drops [68,69]. The frequency of these oscillations is controlled by surface tension and the mass of the drop [70], and viscous forces tend to dissipate these oscillations.

Sheet breakup: In several situations relevant to BPA, the blood spatter originates from a liquid sheet that subsequently experiences several topological changes until it breaks into drops. Complex instability mechanisms drive these topology changes, from sheet to jets, and from jets to drops as shown in Fig. 6. These topology changes are important, because they indicate that there is no such thing as a single "point" of origin of a blood spatter. Sheet breakup has been studied in relation to commercial nozzle and spray generation processes, as reviewed by Lefebvre [71], and also in relation to its occurrence during drop impact (see Section 5.2 and [72]). The breakup of a sheet involves a cascade of events, such as (1) the thickening of the forward edge of the sheet into a cylindrical rim, due to the tendency of interfaces to assume a spatially-uniform curvature, forming either plain cylinders or spherical drops; (2) transverse instabilities on the rim, leading to cusps and finger-like jets; and (3) longitudinal instabilities along the rim, such as the Rayleigh-Plateau [24] instability that break the jets into drops, as in Fig. 6d.

Sheet breakup is more complex than dripping. The time for the sheet to breakup can be estimated using linear stability theory [76,77]. Also, experiments and fluid dynamic models on atomization [78–80] relate the average size of drops to a power of a characteristic Weber number $We = \rho V^2 L/\sigma$, where L is a representative length scale of the initial configuration, for example the thickness of the liquid sheet.

Jet breakup: The formation of drops from a liquid jet occurs by several instability mechanisms that break the jet into a train of drops, as e.g. in Fig. 6d. These mechanisms are reviewed in [23,81]. Instabilities are characterized by their driving and resisting forces, their temporal evolution (growth rate) and their spatial features (wavelength λ). Understanding how instabilities grow helps to determine the time of breakup and the size distribution of the drops.

4. Flight of drops

4.1. Description in the BPA literature

One of the main issues in BPA is to determine *where* a blood spatter originates from, for the purpose of reconstructing the bloodletting event. This operation involves the backward reconstruction of drop trajectories based on the inspection of the stains and on a model for the flight of drops.

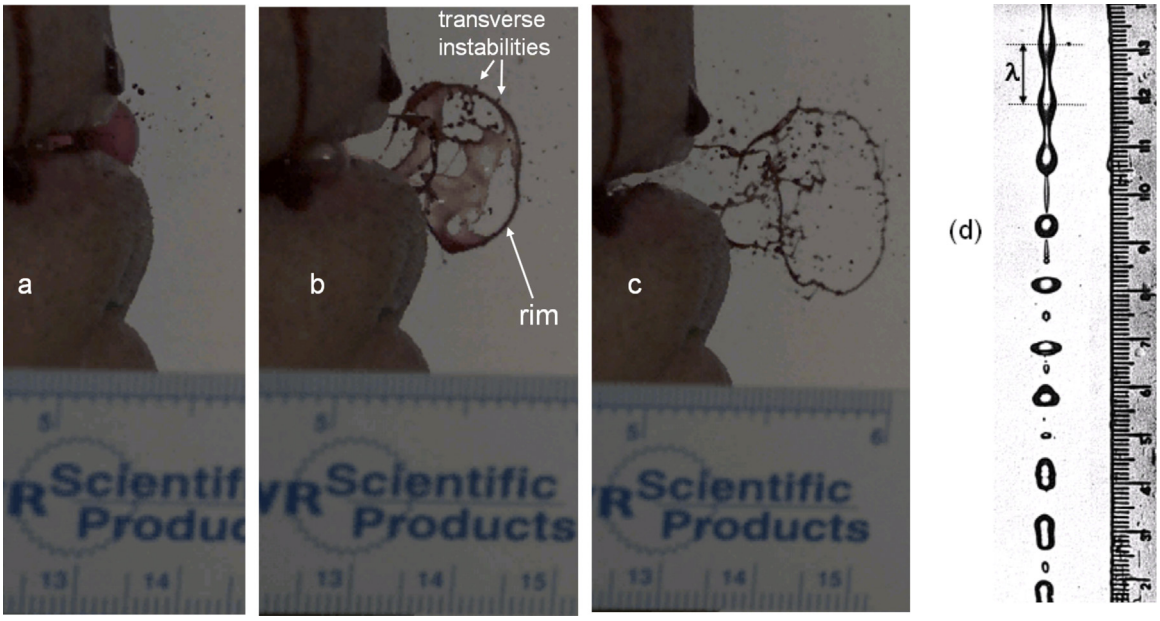

Fig. 6. (a–c) High-speed visualization of the cascade of events leading to the formation of drops during the breakup of a liquid sheet, reproduced with permission from the Midwest Forensic Center [49,73]. Rayleigh-Plateau instabilities tend to minimize surface area and can break a liquid jet into drops, as in picture (d) reproduced from [74,75] with permission from Cambridge University Press.

The traditional terminology used for trajectory reconstruction is illustrated in Fig. 7 and defined in Table 4. The three-dimensional region of origin of a blood spatter is called the *area of origin*, and its normal projection onto a horizontal plane is the *area of convergence*. The area of convergence corresponds to the intersection of straight lines with direction γ, linear projections onto a horizontal plane of the ballistic trajectories of the blood drops. To determine the area of origin, BPA experts use the *angle of impact* α from several stains using the visual inspection methods of Section 5.1. This angle is the acute angle at which a blood drop strikes the target, see Fig. 7b. As an example, in Fig. 7a, the area of origin, target plane and area of convergence are respectively the region near the head of the victim, the floor and the area on the floor supporting the feet of the victim; labeled as α_{1-4} are the angles of impacts of four drops.

An early BPA study on the relation between impact spatters and the area of origin is the graphical work of Piotrowski (1895), extensively reproduced and commented in [82]. The work describes among others the spatial distribution of stains created by a hammer impacting a pool of blood, and the blade of a hatchet hitting either a rabbit head or blood-soaked cotton cloths. Piotrowski observed that the orientation of the stains can indicate the origin of the blood spatter. Both Piotrowski's and Balthazard et al.'s [42,82] work specify that bloodstain trajectories are not straight lines, a concept also reflected in the BPA literature by mention of 'bent trajectories', 'ballistic trajectories' or 'parabolic trajectories', to acknowledge the influence of gravity and drag forces.

As stated in 1939 in Balthazard et al., [42] "*Le problème* [of reconstructing trajectories] *est très difficile à résoudre*". Indeed, reconstructing trajectories is still very difficult today. A first-order approach to reconstruct trajectories is to assume that the droplets travel in a straight line. Reconstruction methods based on straight trajectories, such as the method of strings or the trigonometric

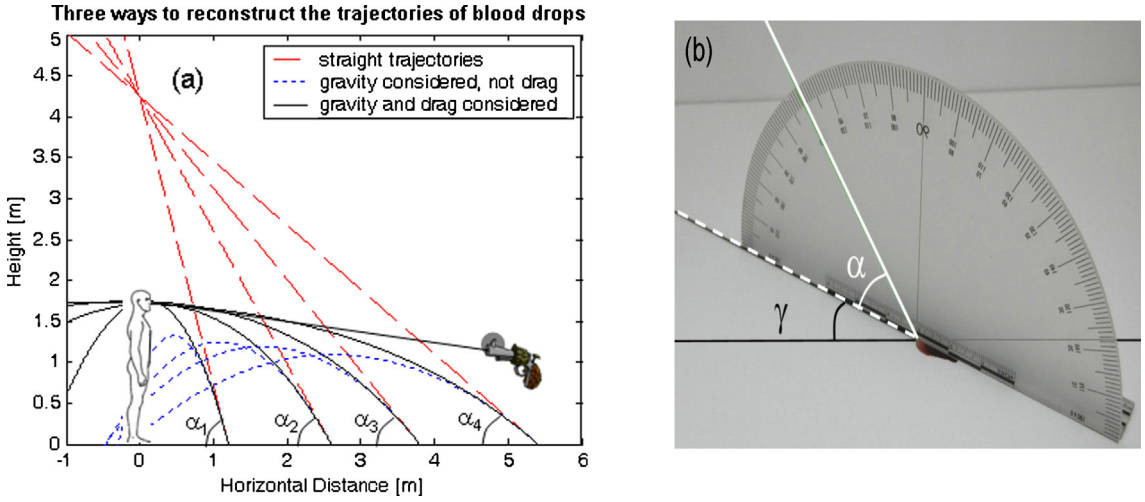

Fig. 7. (a) Reconstruction of the trajectories of four blood drops using straight trajectories vs. ballistic trajectories; the geometry (locations of the four stains, of the victim, impact angles) in (a) is reproduced from teaching material graciously provided by H. MacDonell. Drops size is assumed to be 3 mm, implying velocities in the interval 5.3–7.5 m/s. (b) definition of the angle of impact α and directional angle γ.

method, have been used in crime scene reconstruction since at least the 1950s [83] and have been implemented in software routinely used in crime scenes [84–88]. There is abundant BPA literature on the uncertainties associated with the choice of stains and their inspection to determine the angle of impact and area of origin [89–93]. The uncertainties are of two types, the error induced by assuming linear trajectories, and the uncertainty in determining the angles γ and α from stain inspection. Uncertainty on α has been reported to stem from the asymmetrical nature of bloodstains, the inappropriate use of a protractor [94], or the measurement of the length and width of the stains [95,96]. BPA experts are well aware that the area of origin is determined in an approximate sense [4], either as a maximum height from where the drops could originate, or "*within the volume of a grapefruit, or even a basketball*". This level of accuracy is considered satisfactory for many crime scene reconstruction purposes [4]. Indeed, [97] reports errors on the determination of the region of origin larger than 44 cm due to the assumption of straight trajectories. Similarly verifies experimentally that the stringing method "over-estimates the point of origin and the error associated with this technique is significant (50% on average)." Such error is significant enough to wrongly conclude that a person was standing when in fact they may have been sitting.

Recently, BPA research has proposed methods to reconstruct curved trajectories. Buck et al. [43] reconstructed drop trajectories using ballistic calculations, considering gravity and drag forces. In their ballistic analysis, they screen a range of velocity values for compatibility with the preservation of the drop during the flight (no breakup by drag overcoming surface forces, see Fig. 4). Some assumptions associated with their analysis are discussed in [98]. [99] describes "a method of reconstructing the area of origin in a nonlinear manner", that incorporates the effects of drag into trajectory calculations, using probability densities. Finally, a statistical procedure [100] based on aggregate statistics and the basic equation of projectile motion has been shown to determine the area of origin of a blood spatter for cases when the spatter is launched within a narrow range of polar angles. Since ballistic reconstruction involves the knowledge of impact velocity and drop size (see section 4.2), a significant amount of recent BPA work has focused on obtaining that information by inspecting the stains, as discussed in Section 5.1.

A crime scene can be messy, and stain selection is important in determining the area of origin. Typically, the crime scene investigator selects stains based on the following criteria: accessibility, adhesion to the target surface, abundance, and relative location [97]. Once these stains are chosen, their location is measured, the stains are photographed as a basis to determine their directional and impact angles, so that the areas of convergence and origin of the blood spatter can be determined.

BPA researchers are also aware of two bounds on the velocities of drops: (1) drops will break if drag forces overcome surface tension forces [43], and (2) gravity will not accelerate a drop in still air beyond the terminal velocity [101], which is provided in Fig. 4.

Recent BPA work has identified two limitations of the ballistic reconstruction of trajectories:

1) The area of origin of the drops is distinct from the area of origin of a blood spatter, because the drop generation process involves a sequence of topological changes, such as, for example, during the breakup of a liquid sheet [13].
2) The air through which the drops fly is not always at rest; sometimes the air plays an active role in the transport of drops. In that case, Eq. (1) is still valid to calculate the trajectory, but the velocity used in the related Eq. (2) is the velocity difference between the drop and the air. For instance, experiments involving respiration-caused blood spatters have demonstrated the importance of understanding the role of the surrounding air [102], which helped carrying sub-mm drops further away than occurs in still air.

4.2. Fluid dynamics description

The trajectory of drops has been studied in several applications of a subfield of FD called multiphase flow [58,103–106], relevant for example to spray painting, inkjet printing, fuel injection, meteorology, medical sprays, and the fabrication of micro-particles. Typical topics of interests in multiphase flow are the generation and control of desired distributions of drops size and velocities. The relevant physical parameters and forces are the same as in BPA, the surface tension and viscosity, the drag and gravity forces, and their effects on the drop velocity, shape and temperature. As reviewed in Section 3.2, a wide array of experimental tools are used by the multiphase flow community to characterize the trajectory of drops and of clouds of drops.

Fig. 8 builds on the model problem of Fig. 7, which relates to the reconstruction of ballistic trajectories. For the sake of simplicity, the air is assumed quiescent. In that framework, the trajectories are governed by Eqs. (1) and (2). To solve these equations and reconstruct ballistic trajectories, values of the impact angles, impact velocity and drop size are needed.

Parametric studies in Fig. 8 illustrate how uncertainties on the impact angle, impact velocity and drop diameter influence the determination of the region of origin of that specific blood spatter. To do so, the baseline case (black solid curve) is modified with a typical uncertainty on the impact angles (top right), on the impact velocity (top right) and the drop size (bottom left). The value of the typical uncertainty is set to +/-10%, as it is representative of uncertainties in the measured the impact angle [95,96], the droplet impact velocity [107] and diameter [107], the latter two being determined with the method of spines. For the specific BPA example in Figs. 7 and 8 the largest errors on the determination of the area of origin are shown in Fig. 8d, and come from (in order of the magnitude of the effect): neglecting gravity (error of several meter), neglecting drag, uncertainty on the impact velocity and impact angle, and uncertainty on the diameter of the drop.

Calculations of trajectories are not trivial because flying drops do not behave as rigid particles: they might deform or break up in smaller drops when the drag forces become comparable with the surface tension forces, as explained in Section 2.2.1(b1). Recombination and oscillations might occur during flight, see Section 3.2, affecting the drag, the calculation of trajectories as well as the stain shapes and sizes [19,108,109]. Another concept important for the reconstruction of trajectories is the notion of terminal velocity, described in Section 2.2.1(b3). Also, when droplets are generated at velocities comparable to the speed of sound, e.g. by gunshot, the drag coefficient depends on the compressibility of the air. In that case, correlations used in rocket design could be used [110] for the estimate of the drag force.

It is also important to mention that blood spatters originate from blood at body temperature (37 °C) that typically travels through colder air and impacts a colder target. To the best of our knowledge, the issue of the cooling of the droplet in flight and during impact [111] has never been addressed in the context of BPA, as shown in Table 4. This issue might be important because the physical properties of blood vary considerably: when cooled down from 37 °C to 20 °C (Table 1), the viscosity and surface tension increase by 60% and 27%, respectively. Such large changes of physical properties affect the Reynolds and Weber number, which might affect in-flight atomization, drop spreading, spine formation and splashing.

A related issue is the evaporation of drops during flight, which might be most important for small drops traveling at large velocities, because of their higher surface to volume ratios.

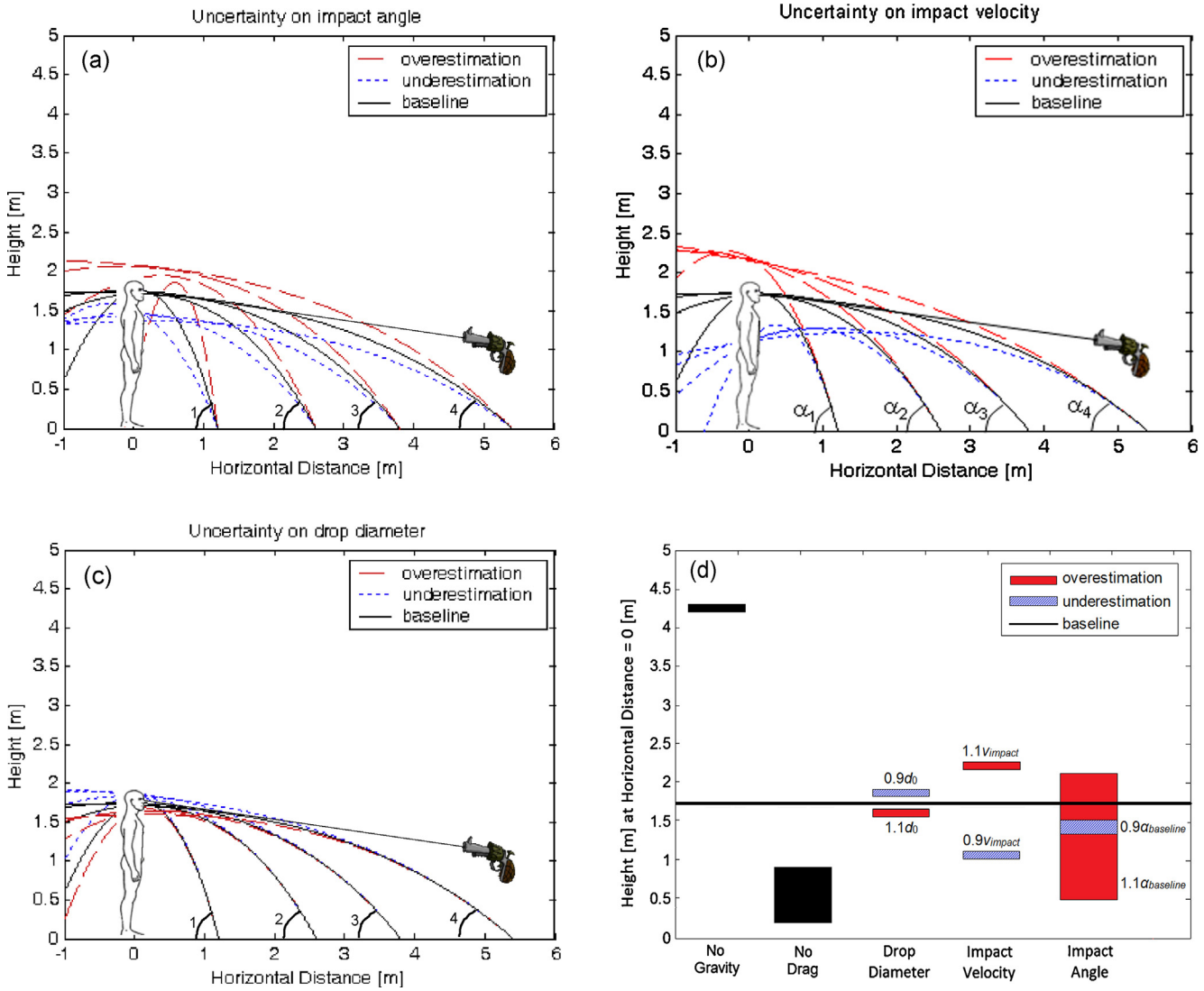

Fig. 8. Examples of how uncertainties on physical parameters influence the determination of the area of origin of a blood spatter: (a) Effect of uncertainty in the impact angle; (b) effect of uncertainty in impact velocity; (c) effect of uncertainty in drop diameter; d) estimated heights of area of origin for initial conditions reported in Figs. 7 and 8. In figures (a–c), the baseline case is the same as in Fig. 7, while a representative error of +10% is assumed for the *overestimation* curve, and of −10% for the *underestimation* curve.

5. Impact

5.1. Description in the BPA literature

As early as 1939, Balthazard et al. [42] pioneered the scientific investigation of drop impact for BPA, investigating experimentally and rigorously how the fall height of a drop influences the shapes of stains, for both normal and oblique impact. These authors took care to discriminate interesting findings from useable findings, and recorded first high-speed movies of blood drop impact. Indeed the relation between the shape of a stain and the impact conditions of the related drop is key for reconstructing trajectories.

As of today, impact is probably the best understood of the four chronological stages described in this review (drop formation, flight, impact and staining). An excellent exposition of the current knowledge in BPA on drop impact is available in the recent review of Adam [14].

Before the early 2000s, the BPA community named the blood spatters in relation to the speed associated with the spatter generation, with the terms of Low, Medium or High Velocity Impact Spatter [5]. The reason was to acknowledge an inverse correlation between the stain sizes and the magnitude of the velocity or momentum applied to the static blood to produce the spatter.

Later, this classification scheme was reconsidered after observing overlapping stain sizes between the Medium and High Velocity categories. A novel taxonomy, with examples in the left column of Table 4, was proposed by The Scientific Working Group for Bloodstain Pattern Analysis (SWGSTAIN, an FBI-founded international group). The taxonomy classifies the stains in three categories [5] based on the mechanisms driving the staining process: *passive stains* are caused by gravity as the only driving force; *spatter stains* are formed by additional forces besides gravity, such as the momentum of an impact, and *altered stains* exhibit the influence of physical or physiological events occurring *after* the staining process, such as cleanup attempts, decomposition or flaking.

Normal impact

When the impact angle $\alpha = 90^\circ$ (see Fig. 7b), the impact is normal to the target. An impact under any other angle is called oblique, and will be treated subsequently as it involves a more complex and asymmetrical deformation of the drop.

Upon normal impact, the contact diameter between the drop and the target surface expands until it reaches a maximum, in a process called *spreading*. In [42], a relation was found experimentally between the height of a drop in free fall, and the diameter of the stain: the higher the fall, the larger the spreading and stain size.

The simplest parameter to characterize the spreading is the *spread factor* d_{max}/d_0, i.e. the ratio of the *maximum contact diameter* over the *initial drop diameter*. The spread factor has been estimated using first-order FD models [13,112–114]. These models compare the various energy terms available before impact (potential, surface, kinetic) with energy terms available after impact, considering that some of the impact energy has been dissipated by e.g. viscous forces. Since spreading is typically driven by inertia and gravity and resisted by surface tension and viscous forces, the spread factor can be estimated with a relation of the kind, $d_{max}/d_0 = f(Re, We, Fr)$, with the dimensionless numbers defined as in Table 2. Arguing that in several cases relevant to BPA, $We >> Re$ and neglecting the effect of gravity during the impact, Chandra's group proposed the correlation [114]

$$\frac{d_{\max}}{d_0} \cong \frac{1}{2} Re^{1/4}. \tag{8}$$

Relations developed with a similar approach are also in [11,115].

By itself, the description of Eq. (8) is of limited use in BPA because the initial diameter of a drop is rarely known; however, the combined measurement of spreading and spines (below) can help estimate the impact conditions.

When the impact energy is large enough, the edge of round stains are no longer smooth, but rather disturbed by *spines* – also called fingers, scallops, sunburst effect [116] or spikes – as shown in Fig. 9a. Spines appear in increasing number as the impact velocity increases [42]. The instability mechanism responsible for the formation of these spines has only been investigated recently. Marmanis and Thoroddsen [117] developed a correlation between the impact Reynolds number and the number of fingers, N, and attributed the fingering to interactions between inertial and viscous forces, see also [118]. Recently, Hulse-Smith et al. [114] proposed a correlation dependent on a target-specific empirical coefficient, $C \sim O(1)$, and on the Weber number, i.e. the ratio of inertial forces (that enhance fingering) to the surface forces (that reduce fingering), where

$$N = C\sqrt{We}. \tag{9}$$

Reference [114] proposes to combine Eqs. (8) and (9) to determine d_0 and v_0 based on the measurement of the stain size d_{max} and of the number of spines N, assuming that the material properties of the blood (ρ, μ, and σ) and of the target material (C) are known. That approach to determine the impact conditions from the inspection of a stain is known as the *method of spines*. A derived approach, independent of the physical properties of the blood, is described in [107] for impacts on paper, drywall and wood. Spines can merge or be indistinguishable from oscillations on the edge of the stain due to local changes of substrate roughness or wettability. As a result, there is an inherent subjectivity in determining the number of spines, leading to recommendation in Hulse-Smith and Illes [107] that only one individual count all the spines related to a specific BPA study. In [14], Adam also mentions two limits of applicability of the *method of spines*: the absence of spines for low-energy impacts and the saturation of the number of spines at high Weber numbers, see Fig. 9b.

The occurrence of *splashing* –the breakup of the drop into distinct amounts of liquid upon impact- can be explained in relation to the formation of spines. Since the formation of the spines is driven by inertia and resisted by capillary and viscous forces, three regimes can be identified in a *Re–We* plane (or in a v_0–d_0) plane. When the ratio of inertia over capillary and viscous forces is low, the drop spreads without scallops nor spines. When that ratio becomes larger, the edge of the stain exhibits spines. When that ratio becomes critically large, instabilities grow to the point of breakup and splashing [118]. Quantitative criteria to discriminate between these three regions are described in [14].

Regarding the influence of the *target*, as documented by Balthazard et al. [42], its shape, material, preparation, structure and oxidation influence the spreading of drops, the formation of spines and of stains. Since most blood drop impact studies have been made on paper, the corresponding published BPA literature is only valid for impacts on paper targets. For instance, Balthazard et al. mention [42] that their results are only valid for impact on a specific type of cardboard paper. In [4,119], MacDonell writes about how the substrate roughness can increase spatter, i.e. promote splashing. Studies [89,114] compare blood drop impact on different substrates (glass, paper, steel and wood), with different roughness. Note also that a specific class of target surfaces is of specific importance for BPA: clothes [120].

A large set of *high-speed visualization experiments* of normal and oblique impacts on various substrates, at various speeds, is available, with the techniques and from the sources mentioned in Section 3.1.

Two *questionable assumptions* sometimes appear in BPA reports on the impact of drops:

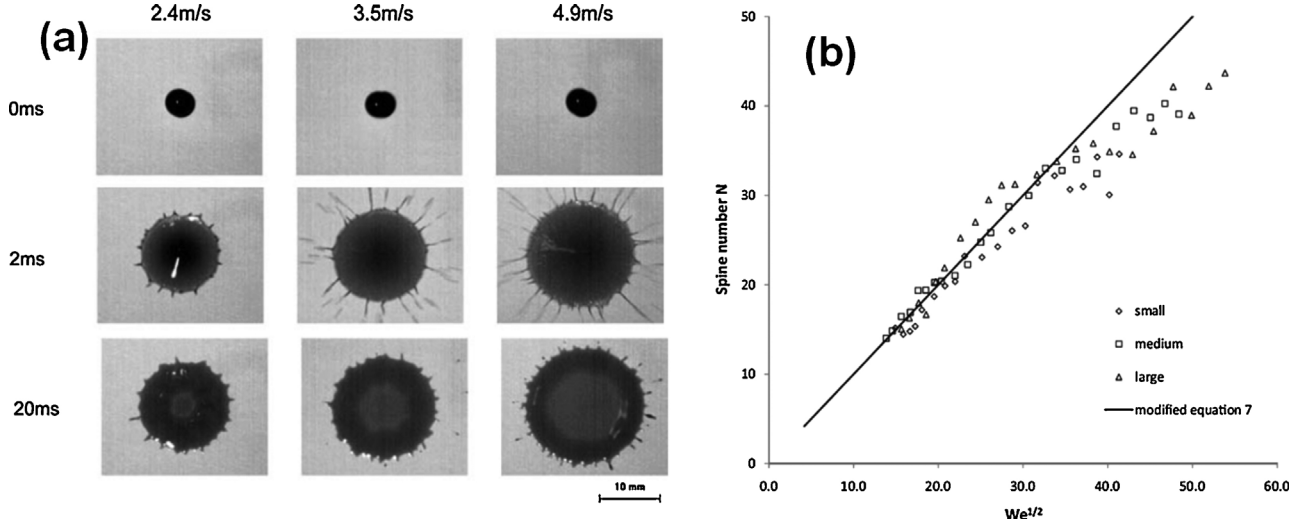

Fig. 9. Fluid Dynamics instabilities tell about the impact conditions. The number of spines radiating from the edge of a stain increases with the impact velocity (a), reprinted, with permission, from [107], copyright ASTM International 100 Barr Harbor Drive, West Conshohocken, PA 19428. In (b), the graph reprinted from [14], Copyright (2012), with permission from Elsevier, shows the dependency of the number of spines on the Weber number.

1) *the stain area corresponds to the maximum contact area between the drop and the target during impact (=maximum spreading).* This is probably realistic for substrates that are hydrophilic, but not for hydrophobic substrates, such as greasy tiles, where the stain diameter can be smaller than the maximum diameter reached during impact, as clearly shown in [42]
2) *the stain diameter indicates the distance of fall* [121], or *the impact velocity*: this is only true if the initial size of the drop is known, as was also clearly shown in [42].

Oblique impact

The oblique impact of drops on a surface is illustrated in Fig. 10, and result in elliptical stains. The lateral spreading W (the minor axis of the elliptic stain, perpendicularly to the projection of the velocity vector on the target) is driven not by the whole velocity, but by the velocity component normal to the surface [14]. An equation similar to Eq. (8) therefore applies, where Re is defined based on the velocity component normal to the surface. The axial spreading, L, along the projection of the impact velocity onto the target plane is typically larger than W: while the velocity component normal to the surface induces axial spreading similarly as the longitudinal spreading, the cylindrical path of the droplet intercepts the surface at an angle α, and this latter contribution makes L larger than W, *so that the stain is elliptical.*

Experiments show that the ratio W/L of the extension in the lateral direction over that in the forward direction increases monotonically with an increasing impact angle [42], following a trigonometric relation first established in [122]

$$W/L = \sin\alpha. \tag{10}$$

Measuring the ellipticity of a stain therefore provides important information on the impact angle. The error using the formula (10) is estimated in [89,121]. Note that elliptic stains do not necessarily imply an oblique impact, as any relative motion of the target perpendicular to the drop trajectory can cause a non-circularity in the observed stain, a fact studied experimentally in [123].

Balthazard et al. described that the impact velocity modifies the shape and number of *spines* at the forward end of a stain resulting from an oblique impact [42]. Knock and Davidson [124] propose an

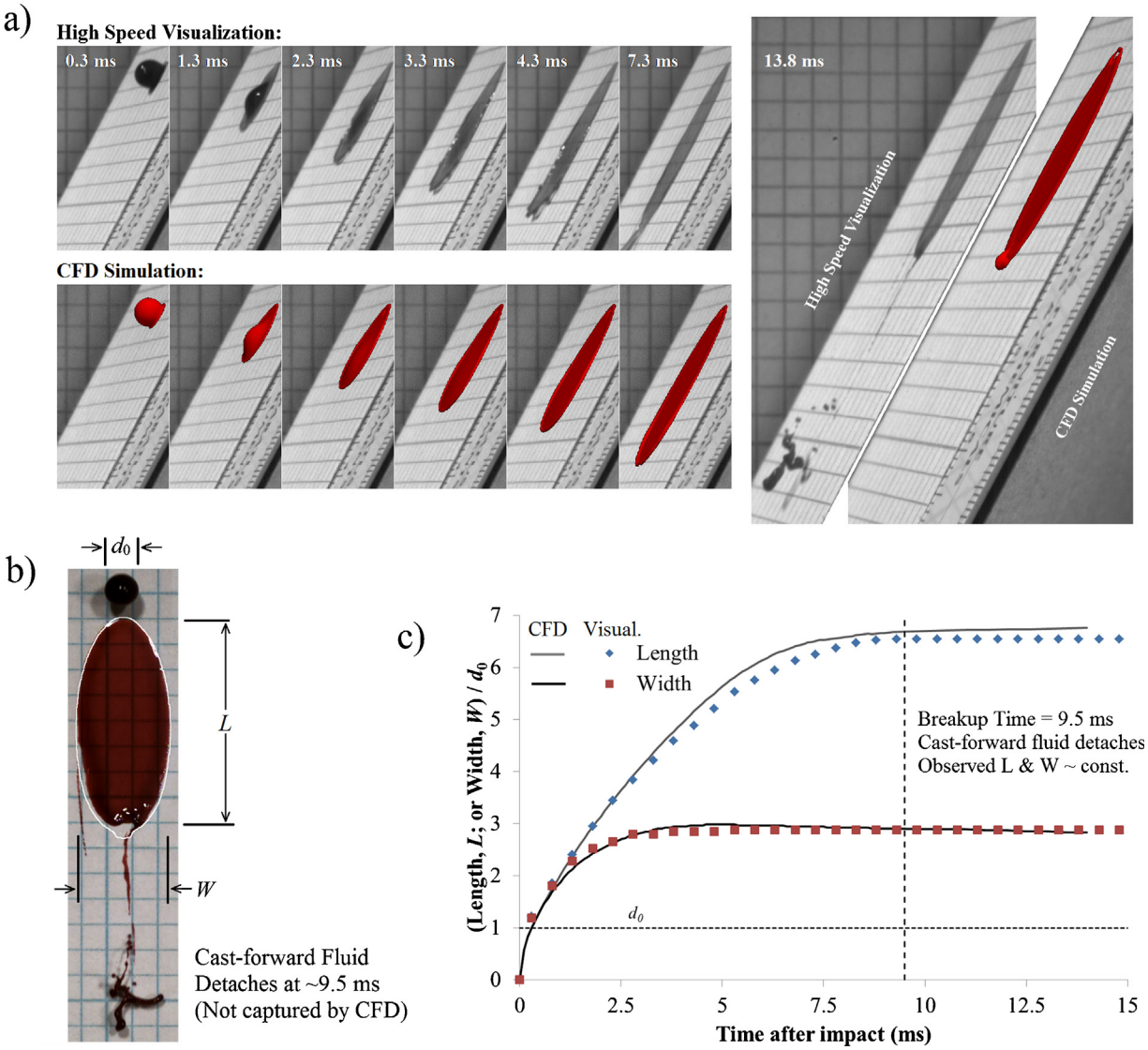

Fig. 10. Experimental and computer-based simulations of the impact of a 4 mm blood droplet striking an oblique surface at 28° and 4.3 m/s: Comparative droplet shapes (a) from high-speed visualization (top and grey) and Computational Fluid Dynamics simulations (bottom and red) for the indicated times after impact; (b) overlay of simulated (white outline) and experimental drop/stain shape prior-to impact and 13.8 ms after impact; and (c) variation with respect to time of L and W. The final experimental W/L elliptical ratio of 0.44 corresponds to $\alpha = 26.1°$ from Eq. (10). Experiments adapted with permission from the MFRC Bloodstain Pattern Analysis Video Collection [50]; simulations from coauthors A.D. and D.A. (For interpretation of the references to colour in this figure legend, the reader is referred to the web version of this article.)

approach to determines d_0 and v_0 by inspection of the bloodstain size and the number of spines for oblique impact.

In relation to *splashing*, Pizzola et al. [41] describe the formation of a *wave-castoff*, this single satellite drop detaching from the forward end of the parent drop during an oblique impact.

Several recent publications on the impact of blood drops have related the outcomes (spine formation, stain diameter and shape) to impact conditions within a dimensionless framework [11,14,114]. For example, Adam [14] proposed that the observed impact behavior of blood droplets (i.e. gentle spreading into a smooth ellipse, appearance of scallops or spines, splashing into several drops) is controlled by the ratio of the inertia of the flow at the wetting line parallel to the target plane, over the stabilizing forces of viscous dissipation and surface tension. A similar theory was verified for Newtonian fluids [125] and explains why, in experiments where the inertia of the impact is gradually increased, scallops, spines and splashes are typically observed at the leading edge of a stain earlier than at the trailing edge.

A misconception concerning oblique impact is that *the stain width equals the drop diameter* [90]. This is not a universal truth as evidenced by $W \gg d_0$ in Fig. 10.

5.2. Fluid dynamics description

Several reviews of the fluid dynamics of drop impacts on liquid and solid surface are available in [126–128]. Upon impact, the fate of a droplet can have various outcomes, such as spreading, splashing, bouncing, or a combination of these. These outcomes are reviewed here considering mostly normal impacts. As the description of impact is quite extensive in the BPA literature, the present section does not repeat what was exposed in details in Section 5.1.

While FD researchers can use the same wide collection of experimental tools to describe drop impact as for drop breakup, there is also a mature FD discipline called *Computational Fluid Dynamics* (CFD), which can be presented as follows. CFD has been widely applied to drop impacts and offers research and teaching opportunities for BPA, as exemplified in Fig. 10. The fundamental equation describing FD phenomena such as the impact of a drop of Newtonian fluid is the Navier–Stokes equation, the expression of Newton's second law, Eq. (1), for fluid flows. Because of its explicit modeling of the viscous dissipation inherent to fluid flows, the Navier–Stokes equation is a non-linear, second-order partial differential equation, quite difficult to solve with pen and paper. CFD methods are computer-based techniques to solve equations such as the Navier–Stokes equations. To do so, the volume (the deforming drop) and the time (for example, from impact to drying) of interest are divided into a large amount of small volumes and small time increments. The Navier–Stokes equations are then discretized, i.e. expressed in an algebraic manner, for each of the small volumes and times, reducing the complex partial differential equations into large numbers of algebraic equations that can be numerically solved with computers.

CFD studies on droplet impact have been reviewed in [127]. These numerical efforts were pioneered by Harlow and Shannon in the 1960s [129]. Subsequent work added the effect of viscosity [130], surface tension [131], wetting [113] and heat transfer during impact [132]. Later, researchers studied numerically the evaporation of drops on solid surfaces, see Section 6.2.

There are currently no simulation tools that solve both the impact of a drop and the formation of a stain, but current simulation techniques are ready to address this challenge. These simulation tools could be used for investigating parameters that are difficult to investigate experimentally, such as the influence of viscosity, substrate wettability, or drop sizes and velocities that are relevant to crime scenes, but difficult to reproduce experimentally.

An example of current capabilities of Computational Fluid Dynamics is shown in Fig. 10a. Input parameters of that simulation are the target wettability and the impact conditions. These preliminary three-dimensional simulations incorporate a dynamic wetting model [133,134]. The simulation of oblique impact of a blood droplet on a paper target shows similar features as the experiments. For example, the simulated evolution of the wetting line, i.e. the motion of the boundary of the stain, closely matches the experimental data.

The spatial and temporal resolutions of the simulation in Fig. 10 are however insufficient to capture the surface instabilities and the subsequent splashing observed at the leading edge of the impacting droplet, visible for times 3 to 10 ms. In that context, it is important to mention that simulations are not a *panacea*, because of the difficulty to model phenomena such as spine formation or wetting, which feature significantly smaller time scales or length scales than the typical scales used in the simulation. CFD simulations are indeed numerical representations of the continuum reality and necessarily partition the time and space with a given *resolution*, in a similar way as a digital picture images the real object with a given resolution of pixels.

To accurately estimate the *spreading* with Eq. (8), the viscosity of the blood needs to be known. In contrast to Newtonian fluids like water and liquid metals, the viscosity of blood is reduced by the high shear rates experienced during the impact process. In fact, during the early stages of the impact, for geometric reasons, the fluid velocities can be orders of magnitude larger than the impact velocity [127]; also, at large Reynolds numbers, the drop spreads into a very thin film surrounded by a donut-shaped ring where fluid accumulates [135]. The combination of large velocities and a thin film induces very large shear rates during the impact, causing the viscosity to decrease significantly. This begs the questions: *what viscosity value should be used to calculate the droplet Reynolds number for describing impact conditions?* This question can be answered as follows. The viscosities provided in Table 1 are for shear rates on the order of several hundred s^{-1}, above which the dependence on shear is somewhat limited, since thinning has already occurred. Considering that most viscous energy dissipation during impact would occur in a thin sheet (length scales below 1 mm), the shear rate would likely be at least on the order of 1 m/s / 0.001 m, or 1000 s^{-1}. It is thus reasonable to assume that the initial droplet spreading characteristics can be described by the high-shear viscosities provided in Table 1. Note that the latter stages of droplet spreading and the staining process occur at much smaller velocities and shear rates, and therefore proceed at much higher viscosity.

In [126], Yarin describes the threshold condition which determines whether the drop spreads or *splashes* upon impact, based on considerations of the physical forces exposed in 5.1.1. Splashing typically occurs after a circular sheet or "corona" is formed [136]. The criterion to discriminate between spreading or splashing is

$$ReWe^2 = K^4. \tag{11}$$

where K is a target-dependent empirical constant, estimated as 57.7 in [136]. The influence of the substrate on the spreading and splashing has been studied in [126,137–141]. Recent research by Nagel's and Brenner's groups has identified that the compressibility of the air surrounding the droplet [142,143] affects the splashing. For typical BPA situations, their results agree with the criterion of Eq. (11).

In 1967, Ford and Furmidge [144] considered the influence of *target* wettability on the impact and spreading of drops. As

discussed in Section 2.2, the target elasticity –even the hardest glass or metal have some degree of elasticity- also influences the splashing. Lesser showed analytically [145] that during impact, the onset of sideways jetting of liquid from beneath the drop will be delayed by an elastic response of the wall, a phenomenon confirmed experimentally [146]. Rein [128] reviews that the elastic response of most surfaces has no influence at low velocities, but becomes important during high-speed impacts.

Importantly, the *wetting angle* (see Fig. 2) is not a constant during impact as described in [133]. The wetting angle is also function of the direction of motion of the wetting line (advancing or receding), and of the relative speed between the wetting line and the substrate (or the capillary number). This dynamic behavior of the wetting angle influences the spreading and is still a topic of current FD research [133,147–150].

Upon impact, the liquid contained in the drop might fully or partially *bounce* away from the wall [126,151–153]. A correlation in [154] predicts the volume of Newtonian liquid that will be retained on a solid surface, based on the difference (or hysteresis) between receding and advancing wetting angles.

The impact of drops on liquid surfaces has been reviewed in [128], and involves the deformation by the impacting drop of the free surface of the liquid into a liquid sheet. That protruding liquid sheet, sometimes in the form of a crown, might break up into drops, by instability mechanisms described in Section 3.2. Impact on liquid surfaces is important for basic FD studies on, for example, the noise of rain, and also for drip patterns in BPA.

6. Staining

This section focuses on how the stain forms, after the impact has deformed the drop. In other words, non-inertial aspects of the fluid transport are discussed, since inertial aspects (spread factor, impact angle, fingering, splashing) associated with the impact have already been discussed.

6.1. Description in the BPA literature

The *uneven thickness* of stains was described by Balthazard et al. [42], who noticed that the periphery of stains is typically thicker than their center. The authors guessed (rightly as shown in the late 1990s [155]) that the depressed center is rather due to some phenomenon occurring during the drying phase rather than to the presence of air bubbles in the impacting drop. The same work [42] commented on the presence of scale-like structures in the crust of the stain, and noticed that the appearance of the crust depends on the type of blood used, either real blood or blood with anticoagulant. They also mentioned that stains resulting from oblique impact are inhomogeneous, the bottom part being "crust-like" and dark, while the upper part is pink.

Balthazard et al. [42] also studied how *capillary forces drive blood into fabrics*, noticing faster imbibition rates along the fibers than across. Kirk [120] also notes that some bloodstains go straight from the generation to the staining phase, describing the case of a stabbed woman whose blood had flowed between her breasts and into her clothing.

During drying, stains might suddenly detach from certain targets. This *alteration* process called delamination or warping is caused by radial stresses due to the shrinkage of the stain, which overcome adhesive forces between the blood and target. This effect occurs on smooth plastic sheets, but not on some rougher plastics as described in [42]. Another alteration process is described in the fascinating study [157] on how insects modify the shape of existing bloodstains or create artifact bloodstains.

Kirk [120] also describes methods to *identify* if a bloodstain comes from the perpetrator or from the victim (a question resolved later by genetic testing), as well as methods to spot bloodstains on backgrounds where stains do not stand out. Several chemical, physical or optical methods have recently been developed in BPA for detecting weakly visible stains, using functionalized nanoparticles [158] or Raman scattering [159], and for determining the age of bloodstains, as reviewed by Bremmer et al. [160].

6.2. Fluid dynamics description

Blood is not only a fluid containing particles (complex fluid), it is also a fluid initiating coagulation as soon as it flows out of the human body. Once the kinetic energy associated with the impact has dissipated, the formation of a stain on a solid, impermeable target, depends on the following physical processes: wettability [161], evaporation, viscous dissipation, diffusion and coagulation. Reference [162] discusses the relationship between the rheology of the blood and the stages of blood clotting. Reference [12] describes the effects of various anticoagulants on the trail length left by a drop running along an inclined surface.

The formation of stains during the drying of complex fluids has recently become the focus of fluid dynamics studies motivated either by the ubiquity of this natural phenomenon, or by manufacturing applications of evaporative self-assembly. For instance, the formation of rings at the periphery of stains has been explained in [155] by the combination of a radial flow driven by enhanced evaporation at the wetting line, and pinning of the same wetting line by accumulation of particles carried by the radial

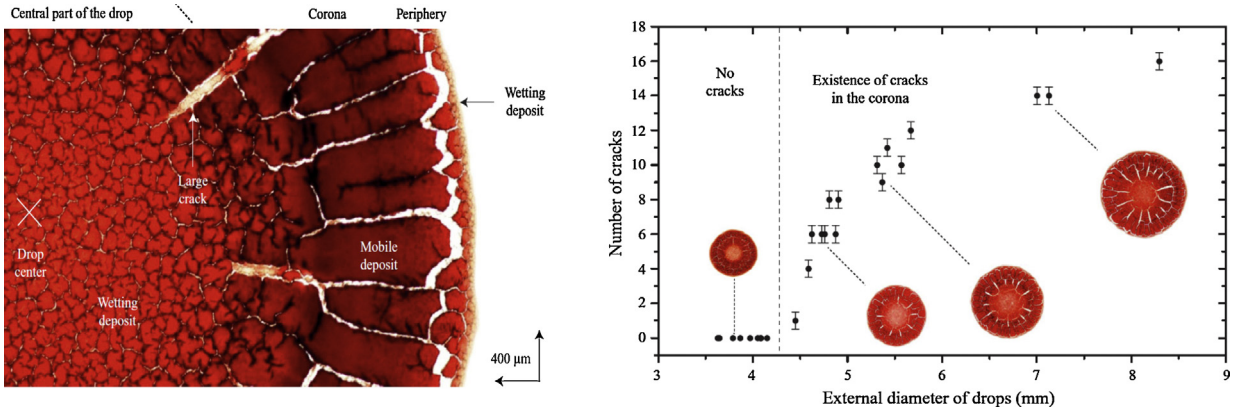

Fig. 11. A magnified stain reveals a wealth of features; some of these features, such as cracks in the corona, are of interest to determine the impact or drying conditions. Images from [156], reproduced with permission from Cambridge University Press.

flow. The evaporation of a drop of a complex fluid such as blood is a typical multiphase process, featuring a *cascade of dimensional transport phenomena*: wetting at the *(1D)* wetting line drives the motion of the *(2D)* solid-air interface, where surface stresses due to chemical or thermal non-equilibrium such as Marangoni stresses [97] drive the bulk flow *(3D)* inside the drop. Several fluid dynamic studies have addressed either experimentally or theoretically the interplay of transport phenomena during drop drying and stain formation [163,164]. For instance, Hu and Larson [165,166] modeled the evaporation of a drop of pure liquid with a pinned wetting line. Simulations of the formation of stains have recently been performed [167–170]; this requires solving the motion of the liquid and of many suspended solid particles. This is a non-trivial task, because of, for example, the interaction of the particles with the wetting line [170].

The formation of stains on porous targets like fabrics and garments involves the additional complexity of *imbibition*. Imbibition is the transport of blood into the fabric, driven by wetting forces and resisted by viscous forces. For one-dimensional imbibition, for example the imbibition of a large cloth dipped normally into a pool of blood, the wetted length evolves as the square root of the time [171]. Some analytical results for more

Table 4a
Definition of concepts relevant to BPA, adapted from the terminology working group of SWGSTAIN.

Stain size	Diameter of a circular stain; length and width for an elliptical stain.
Accompanying drop	A small blood drop produced as a by-product of drop formation.
Altered stain	A bloodstain with characteristics that indicate a physical change has occurred.
Angle of impact	The acute angle (alpha), relative to the plane of a target, at which a blood drop strikes the target. At low impact angles a wave castoff (tiny splashed drop) is released from the main drop in the direction of impact).
Area of convergence; directionality	The area containing the intersections generated by lines drawn through the long axes of individual stains that indicates in two dimensions (in a horizontal plane) the projected location of the blood source; The characteristic of a bloodstain that indicates the direction blood was moving at the time of deposition.
Area of origin	The location in a 3-dimensional space from which the spatter originated.
Backspatter pattern; forward spatter pattern	A bloodstain pattern resulting from blood drops that traveled in the opposite direction of the external force applied, associated with an entrance wound created by a projectile; A bloodstain pattern resulting from blood drops that traveled in the same direction as the impact force.
Blood clot	A gelatinous mass formed by a complex mechanism involving red blood cells, fibrinogen, platelets, and other coagulations factors.
Bloodstain pattern	A grouping or distribution of bloodstains that indicates through regular or repetitive form, order, or arrangement the manner in which the pattern was deposited.
Bubble ring; expiration pattern	An outline within a bloodstain resulting from air in the blood; A bloodstain pattern resulting from blood forced by airflow out of the nose, mouth, or a wound.
Cast-off pattern; cessation cast-off pattern	A bloodstain pattern resulting from blood drops released from an object due to its motion; A bloodstain pattern resulting from blood drops released from an object due to its rapid deceleration.
Directional angle	The angle (gamma) between the long axis of a spatter stain and a defined reference line on the target.
Drip stain; drip trail	A bloodstain resulting from a falling drop that formed due to gravity; A bloodstain pattern resulting from the movement of a source of drip stains between two points.
Edge characteristic; parent stain; satellite stain; fingering; splash pattern	A physical feature of the periphery of a bloodstain; a bloodstain from which a satellite stain originated. A smaller bloodstain that originated during the formation of the parent stain as a result of blood impacting a surface; Formation of spines at the edge of a stain; A bloodstain pattern resulting from a volume of liquid blood that falls or spills onto a surface.
Perimeter stain	An altered stain that consists of the peripheral characteristics of the original stain.
Flow pattern	A bloodstain pattern resulting from the movement of a volume of blood on a surface due to gravity or movement of the target.
Impact pattern	A bloodstain pattern resulting from an object striking liquid blood.
Insect stain	A bloodstain resulting from insect activity.
Mist pattern	A bloodstain pattern resulting from blood reduced to a spray of micro-drops as a result of the force applied.
Serum stain	The stain resulting from the liquid portion of blood (serum) that separates during coagulation.
Spatter stain	A bloodstain resulting from a blood drop dispersed through the air due to an external force applied to a source of liquid blood.
Swipe pattern; transfer stain	A bloodstain pattern resulting from the transfer of blood from a blood-bearing surface onto another surface, with characteristics that indicate relative motion between the two surfaces; A bloodstain resulting from contact between a blood-bearing surface and another surface.
Drip pattern	A bloodstain pattern resulting from a liquid that dripped into another liquid, at least one of which was blood.
Saturation stain	A bloodstain resulting from the accumulation of liquid blood in an absorbent material.
Wipe pattern	An altered bloodstain pattern resulting from an object moving through a preexisting wet bloodstain.
Projected pattern	A bloodstain pattern resulting from the ejection of a volume of blood under pressure.
Deposit volume	The volume of a stain.

complex geometries are referenced in [172]. Reference [173] discusses the effect of surfactants on the ability of a liquid to spread into a fabric.

The formation of *cracks* on stains has been studied in [174]: Allain and Limat showed that the spacing between the cracks was controlled by the competition between the mechanical relaxation due to the opening of a crack, and the increased mechanical stress due to the enhanced evaporation across the walls of the crack. Brutin et al. ([156], Fig. 11) propose a relation between the density of cracks in the crown and the initial drop volume.

7. Synthesis of the relationship between BPA and FD concepts, summary table and research opportunities

Section 2 described the body forces and surface forces at play in the FD of BPA. All these forces are proportional to some physical properties of the blood and/or the target, such as surface tension, viscosity, density, or wettability. It is therefore important to have accurate measurements of these physical properties. Also, while most BPA studies assume typical values for the physical properties, the blood of individuals has properties within a range of values. A cyclist competing for the *Tour de France* typically has more viscous blood, richer in hematocrit [175,176], than an average person. Therefore, studies could be performed to (1) assess the uncertainty involved in using typical physical properties; and (2) refine BPA methods to consider the physical properties of the specific protagonists identified in the bloodletting event. Precise knowledge of, for example, the viscosity and surface tension of the blood spilled at a crime scene might reduce the uncertainty associated with BPA.

A related and specific issue in BPA is that freshly drawn human blood potentially carries pathogens, so substitutes to human blood have been sought since early BPA studies [42] for the purpose of improving the safety of BPA research and teaching. As a result, research opportunities exist in BPA for the development or characterization of substitutes to fresh human blood, such as animal or synthetic blood.

Section 2 also describes an opportunity for the elaboration, publication and dissemination of regime maps that describe aspects of BPA within a dimensionless framework, with ratios of forces. Such maps could characterize the flight or breakup of drops (as in Fig. 4), impact outcomes, and transformations during drying.

Section 3 reviews several aspects of the fluid dynamics of drop generation relevant to BPA. Importantly, high-speed measurements show that in several situations relevant to BPA the drops are not generated at a single point in space, but rather at the breakup location of an initial jet or liquid sheet, protruding from the area of origin of the blood spatter [13], during a cascade of events with specific temporal duration and spatial extension. This cascade of events needs to be understood, modeled as simply as possible and considered for the reconstruction of ballistic trajectories. In that context, there is also an opportunity for models and experiments that link the kinematics of the bloodletting event to the size and speed of the generated drops, as described in Section 3.2.

While the breakup of jets and sheets has been widely investigated in FD, some drop generation mechanisms (gunshot and cast-off spatters) are specific to BPA and might benefit from systematic FD studies. Section 4 reviews FD and BPA studies on the flight of drops. A full backward modeling of the ballistic trajectories of droplets is not yet available for the BPA practitioner. This possibly implies significant uncertainties on the determination of the area of origin. In that context, it would be useful to the BPA practitioner to have a simple method to discriminate between spatters that are suitable for the stringing method and the ones that call for ballistic trajectories.

Also, the accurate reconstruction of curved trajectories (Figs. 7 and 8) relies on the development of reliable methods to estimate the following variables explicitly: impact velocity, impact angle, and impacting drop size.

To the best of our knowledge, a framework is missing for the reconstruction of trajectories in non-quiescent air, such as gunshot spatters, injuries in windy conditions, or expirated spatters. Necessarily, that framework will involve solving the coupled problem of the airflow and the drop flight, a problem that is routinely solved in e.g. the design of fuel injectors. That example suggests that significant untapped expertise is available in the multiphase flow community, in terms of experimental, theoretical and numerical tools.

Section 5 reviews BPA and FD studies on the impact of drops, and describes the potential of computational fluid dynamics to study drop impact cases that are difficult to reproduce

Table 4b
Definition of concepts relevant to FD, from the authors.

Rheology	Relationship between the rate of deformation and the mechanical stresses in a fluid.
Surface tension	Measure of the surface energy between two immiscible materials.
Substrate wettability	Affinity of a solid substrate with a pair of immiscible fluids along it.
Substrate roughness	Average amplitude and wavelength of height fluctuations on a surface.
Substrate elasticity	Ratio of the deformation of a solid surface to an applied normal force.
Dripping	Generation of a drop when gravity overcomes wetting forces.
Jet/sheet generation	Generation of a cylindrical (jet) or planar (sheet) volume of fluid, typically by inertial forces.
Jet/sheet breakup	Separation of the jet or sheet into unconnected liquid volumes such as drops or threads. Breakup is typically driven by instability formation and growth.
Trajectories	Motion of an object in a three-dimensional space, as a function of time.
Drag	Resistance to the flight of a drop, due to the inertia and friction of the surrounding fluid.
Pre-impact oscillations	Time-periodic shape changes during flight, i.e. between the generation and the impact.
Spreading	Deformation of a drop contacting a surface, without breakup in unconnected volumes.
Impact instabilities (fingers, hydraulic jump)	Changes of shape and velocity of the impacting liquid, growing with time at an exponential rate.
Bouncing/Rolling/sliding	During impact, a drop can rebound from the surface (bouncing). An oblique impact that results in motion parallel to the surface, without retention on the surface, is described as rolling or sliding.
Splashing	Deformation of a drop contacting a surface, involving breakup into unconnected liquid volumes.
Imbibition	Transport of a fluid in a porous material, driven by capillary forces and resisted by viscous forces.
Evaporation	Shrinkage of a drop by phase transformation of the liquid into vapor, in an endothermic process.
Phase change (coagulation)	Chemical transformation of the liquid blood into an interconnected network, with solid-type behavior.
Heat transfer	Transport of heat by conduction, convection or radiation.
Mixing	Transport of two species by random molecular motion (diffusion), or by the global motion of a fluid (convection).

Table 4c
Relations between BPA (rows) and FD concepts (columns), with related references in the cells. Colors indicate the type of relation (non-existent, accidental or weak, essential or strong). Inferences obtained from investigating BPA objects are indicated in the second column.

Relations between Bloodstain Pattern Analysis (rows) and Fluid Dynamics (columns) Unknown Relation No Relation Accidental Relation Essential Relation		Property	Rheology Surface tension	Substrate wettability Substrate roughness	Substrate elasticity	Dripping	Jet/sheet generation; Jet/sheet breakup	Trajectories	Drag	Spreading	Impact instabilities (fingers, hydraulic jump); splashing	Bouncing/rolling/ sliding	Imbibition	Evaporation	Phase change (coagulation)	Heat transfer
Object investigated	Inference															
Stain size	*Impact conditions, weapon*		[107,113, 114,131, 139,182, 183]	[42,113, 114,126, 133,134, 140,184, 185]		[61,62]	[5,23, 35,50, 56–58,71, 72,76, 78–81, 103–106]	[11,57, 60,107]	[5,35–37, 186]	[13,107, 112–114, 126–128, 187]	[126–128].	[154]	[42]		[170]	[70, 132, 177]
Accompanying Drop			[62,63, 64]			[61,62, 66]					[142]					
Altered Stain	*aging, wipe*			[42,188]									[188]	[174]	[160, 174]	
Angle of Impact	*area of origin*						[13,19, 68,69, 108,109]	[5,83, 89,90, 91,92, 93,97, 121,122, 123,189]		[14,60, 123]	[11,14, 60,94, 123,125]					
Area of Convergence, Directionality							[13]	[5,97]								
Area of Origin							[13,19, 68,69, 108,109]	[9,11,89, 90,95,98, 121,190]	[15,35, 36,42, 99,186]		[14]					
Backspatter Pattern; Forward Spatter Pattern	*area of origin, weapon*						[46]	[5,45,110, 191]								
Blood Clot			[6,162]												[160, 162]	
Bloodstain pattern	*area of origin, weapon*		[13,35,76]					[13,40,82]	[36,186]							
Bubble Ring; Expiration Pattern	*expiration pattern*		[81,186]					[102]								
Cast-off Pattern; Cessation Cast-off Pattern	*motion, weapon, area of origin*							[5]								
Directional Angle	*Area of convergence*															
Drip Stain; Drip Trail	*height of origin; source-target relative motion*		[64,114, 126,192]	[114,142, 192]		[61,62]		[114]	[5,101, 114,193]		[14]					
Edge Characteristic; Parent Stain; Satellite Stain; Fingering; Splash Pattern	*impact conditions: drop size, impact speed;*		[114,126, 136,142]	[4,42,89, 114,119, 136,142]	[25,27, 128, 146]			[5,11, 114,118]			[14,42, 60,72, 76,107, 114,118, 128,142, 144,182, 194,195]	[154]		[42, 165–170]		[165, 166, 170]
Perimeter Stain	*time between drip and wipe-off,*		[155,196, 197]	[155,188]									[188]	[155,163, 196,197]		
Flow Pattern			[12,162, 198]	[12,162, 185,198]						[185]					[12]	
Impact Pattern	*weapon, motion; directionality*		[78–80, 128]					[5]			[72,128, 136]					
Insect Stain			[157,199]													
Mist Pattern	*weapon, directionality*		[81,154, 186]				[56–58]	[45,102]	[45,102, 110]							
Spatter Stain									[200]			[126, 151–153]				
Swipe Pattern	*motion, weapon*		[173,199]													
Drip Pattern	*height of origin*		[64,65,126, 128,137]			[61,62]					[72] [136, 137]					
Saturation Stain	*side of cloth, staining mechanism (transfer, impact, contact)*		[21,199, 201]	[21,42,120, 199,201]									[21,42, 120, 201]			
Wipe Pattern; Transfer stain	*motion, weapon*															
Projected Pattern			[23]					[45,191]	[45,191]							
Deposit Volume			[60,62]				[35,76]							[156,174]		

experimentally, involving, for example, small drops traveling at high speed after a gunshot spatter. Related experiments are inherently difficult, in terms of measuring the ratios of drop sizes over stain sizes, or of characterizing how a cloud of drops travels at velocities on the order of 100 m/s.

The flight, impact and drying of blood drops is typically a non-isothermal process, since the blood is spilled at ~37 °C and the air and target surface are at lower, room temperature. The resulting heat transfer modifies the physical properties of the drop significantly [70,177], as described in Section 4.2, with possible consequences on the amount of spreading during impact (see Table 4), or on the stain formation, as has been shown for the field of maskless manufacturing [111]. Heat transfer analyses of drop impact can either be done analytically or via numerical simulations coupling heat transfer equations with the fluid dynamics equations.

There is also no general theory describing the influence of the target (e.g. roughness, permeability, wettability) on the spreading, fingering and splashing process. Specifically there is no simple model for dynamic wetting, although several approaches have been developed recently [24,147,178–180].

Section 6 reviews FD and BPA studies on the formation of stains. Little work has been done on the timing of drying processes, which possibly could tell about the chronology of the bloodletting events. As investigated by Herb MacDonell [181], the growing ring forming at the edge of bloodstains is more adherent to the target than the center of the stain so that wiped-off bloodstains can be used to estimate the time between the staining and wipe-off event. Also, blood drops contain a specific ratio of liquid to solids, and three-dimensional measurements of stains are likely be correlated with the drop volume, a parameter relevant to the reconstruction of ballistic trajectories. To the best of our knowledge, another open problem would be to determine physical criteria for delamination.

A synthesis of the relations between FD and BPA is provided in Table 4c. This table shows the type of relationship between BPA concepts (rows, defined in Table 4a) and FD concepts (columns, defined in Table 4b), with colors indicating the type of relationship between the concepts. Table 4c also expresses the type of relation (non-existent, accidental, essential). When available, key references from the literature are provided for individual cells of the table.

8. Conclusion and epilogue

This manuscript has highlighted some key relationships between the disciplines of bloodstain pattern analysis (BPA) in forensics and that of fluid dynamics (FD) in the physical sciences. The body of knowledge related to drop generation, drop flight, drop impact, and stain formations has been presented as it is known in the BPA and FD communities. Tables 1 and 2 summarize key physical properties and parameters relevant to BPA, with their typical values. Novel material has been proposed demonstrating the use of dimensionless numbers (Figs. 3 and 4), assessing the importance of parabolic trajectories (Figs. 7 and 8). The intent of this work is to help build bridges between the BPA and FD communities, expanding and refining the many existing connections summarized in Table 4c. Also, in the context of the 2009 report of the US National Research Council advocating for stronger scientific foundations in BPA, several opportunities for joint research between BPA and FD have been mentioned.

Regarding the crime scene in Fig. 1, the BPA analyst and coauthor C.M. proposed the following interpretation after a BPA analysis. The victim suffered multiple stab wounds and was left lying on the floor. During that time, blood pools on the kitchen floor (Area AE in Fig. 1). Then, the victim stands up using the stove for support, probably causing with his arm the flow (AA) and transfer patterns (AB) on the stove. Standing still, blood drips causing the drip stain pattern (AD). Then the victim walks towards the living room, and is attacked again in the hallway. Several elliptical stains (B) on the hallway wall can be used to determine the area of origin of the resulting spatter. Can we expect joint future FD and BPA research to help refine this interpretation? Probably. Research on atomization mechanisms might clarify the causes of spatter B, be it for instance a beating or a stabbing. Research on ballistic reconstruction of trajectories might improve the determination of the area of origin of spatter B. Research on the drying of stains might help telling when the pool AE formed, and how much time elapsed before the victim stood up, forming the associated drip patterns AD.

Acknowledgements

The authors acknowledge financial support from Iowa State University, the US National Institute of Justice (award 2010-DN-BX-K403) and the US National Science Foundation (award CBET 1211187). Several undergraduate and graduate students at Columbia and Iowa State University have participated to the early stages of the literature review, Max Gilmore, Martin Li, Seth Aaron, Junfeng Xiao, Liqun Fu, Ashish Shah and Ying Xing. D.A. acknowledges that Herb MacDonell and then David Baldwin have introduced him to the challenges involved with BPA. D.A. is thankful to have been able to read reference [42] in his mother tongue. This solid and enlightening introduction to BPA deserves a better English translation.

Appendix A. Calculations of the various integrals presented in Section 2.2.1

In this appendix we provide exact expressions of the integrals defined in Section 2.2.1. Note that the trajectories are along a vertical z-axis oriented upwards, with the target at $z = 0$ and the release of the drop at a height $z = h$.

In Eq. (6), the ratio Δ of the work of the drag force W_D over the initial kinetic energy E_{k0} can be calculated numerically with the following integral

$$\Delta = W_D/E_{k0} = \frac{\int_h^0 F_D dz}{\frac{1}{2}mv_0^2} = \frac{\int_h^0 \frac{1}{2}\rho_a C_D A_d v^2 dz}{\frac{1}{2}mv_0^2} = \frac{3\rho_a \int_h^0 C_D \left(\frac{dh}{dt}\right)^2 dz}{2d_0\rho_L v_0^2} \quad (12)$$

where h is the height of the fall, and the drag force F_D is a function of the local velocity, as per Eqs. (2) and (3). The term left in the integral of Eq. (12) needs to be calculated by numerical integration of the trajectories.

In Eq. (5), the ratio of the gravity work W_g over the initial kinetic energy E_{k0} can be calculated from the initial conditions

$$G = \frac{\int_h^0 -mg\,dz}{\frac{1}{2}mv_0^2} = \frac{2gh}{v_0^2} \quad (13)$$

In Eq. (7), the ratio $\Gamma = mg/F_D$ of the weight over the drag force can be expressed and simplified as

$$\Gamma = \frac{mg}{F_D} = \frac{4\rho_L d_0 g}{3C_D\rho_a v_0^2} \quad (14)$$

Appendix B. How to use of impact velocity plot in Section 2.2.1, Fig. 4

Steps to determine the impact velocity from known initial velocity v_0 and initial diameter d_0, using Fig. 4:

Input d_0 on horizontal axis.

Move vertically until crossing the violet curve: the terminal velocity $v_{terminal}$ is found on the violet vertical axis, right, at the same vertical level.

Identify ratio $v_0/v_{terminal}$ of the initial velocity over terminal velocity on the vertical axis, left.

The ratio of impact velocity over terminal velocity is determined by the contour value at the intersection of the vertical line passing by d_0 and the horizontal line passing by $v_0/v_{terminal}$.

Example (shown by capital letters in Fig. 4):

Step\example	*A*	*B*	C
v_0	3.5 m/s	50 m/s	0 m/s
Step 1: d_0	0.2 mm	4 mm	4 mm
Step 2: $v_{terminal}$	≈ 0.7 m/s	≈ 10.3 m/s	≈ 10.3 m/s
Step 3: $v_0/v_{terminal}$	≈ 5	No value, as drop breaks up into smaller drops	0
Step 5: $v_{impact}/v_{terminal}$	≈ 1.0		≈ 0.4
Step 5: v_{impact}	≈ 0.7 m/s		≈ 4.1 m/s

References

[1] T. Bevel, R.M. Gardner, Bloodstain Pattern Analysis with an Introduction to Crime Scene Reconstruction, CRC Press, Boca Raton, FL, USA, 2008.
[2] O. Darrigol, Worlds of Flow: A History of Hydrodynamics from the Bernoullis to Prandtl, Oxford University Press, 2005.
[3] "Strengthening Forensic Science in the United States: A Path Forward", Committee on Identifying the Needs of the Forensic Sciences Community, National Research Council, 2009.
[4] H.L. MacDonell, Bloodstain Patterns, 2nd ed., Laboratory of Forensic Sciences, Corning, NY, USA, 2005.
[5] S.H. James, P.E. Kish, T.P. Sutton, Principles of Bloodstain Pattern Analysis: Theory and Practice, CRC Press, 2005.
[6] I. Anadere, H. Chmiel, H. Hess, G.B. Thurston, Clinical blood rheology, Biorheology 16 (1979) 171–178.
[7] B.A.J. Larkin, M. El-Sayed, D.A.C. Brownson, C.E. Banks, Crime scene investigation III: exploring the effects of drugs of abuse and neurotransmitters on Bloodstain Pattern Analysis, Analytical Methods 4 (2012) 721–729.
[8] M.J. Sweet, Velocity measurements of projected bloodstains from a medium velocity impact source, J. Can. Soc. Forensic Sci. 26 (1993) 103–110.
[9] A. Pace, A.L. Carter, C. Moore, B. Yamashita, Another Treatment of Three-Dimensional Bloodstain Pattern Analysis, Int. Assoc. Bloodstain Pattern Analysts News 22 (2006) 4–11.
[10] B. Brinkmann, B. Madea, S. Rand, Influencing factors of blood stain morphology, Beitr. Gerichtl. Med. 44 (1986) 67–73.
[11] C. Knock, M. Davison, Predicting the position of the source of blood stains for angled impacts, J. Forensic Sci. 52 (2007 Sep) 1044–1049.
[12] J. Finsterer, C. Stöllberger, A. Hochfellner, A. Dossenbach-Glaninger, P. Hopmeier, Factors influencing the length of a blood trail, Haemostasis 29 (1999) 353–354.
[13] N. Behrooz, L. Hulse-Smith, S. Chandra, An Evaluation of the Underlying Mechanisms of Bloodstain Pattern Analysis Error, J. Forensic Sci. 56 (2011) 1136–1142, N. Behrooz, "Bloodstain Pattern Analysis for Determination of Point of Origin," B.S. Thesis, University of Toronto, Toronto, Canada, 2009.
[14] C.D. Adam, Fundamental studies of bloodstain formation and characteristics, Forensic Sci. Int. (2012).
[16] S.D. Gruttola, K. Boomsma, D. Poulikakos, Computational simulation of a non-Newtonian model of the blood separation process, Artif. Organs 29 (2005) 949–959.
[17] R.E. Wells, E.W. Merrill, H. Gabelnick, Shear rate dependence of viscosity of blood: interaction of red cells and plasma proteins, Trans. Soc. Rheol. 6 (1962) 19–24.
[18] L. Langstroth, Blood viscosity. I. Conditions affecting the viscosity of blood after withdrawal from the body, J. Exp. Med. 30 (1919) 597–606.
[19] M. Raymond, E. Smith, J. Liesegang, The physical properties of blood – forensic considerations, Sci. Justice 36 (1996) 153–160.
[20] J. Rosina, E. Kvasnak, D. Suta, H. Kolarova, J. Malek, L. Krajci, Temperature dependence of blood surface tension, Physiol. Res. 56 (2007) S93–S98.
[21] J. Bear, Dynamics of Fluids in Porous Media, Dover, 1988.
[22] S. Charm, G. Kurland, Viscometry of human blood for shear rates of 0–100000 s^{-1}, Nature 206 (1965) 617–618.
[23] J. Eggers, E. Villermaux, Physics of liquid jets, Reports on Progress in Physics, vol. 71, 2008.
[24] P. deGennes, F. Brochart-Wyart, D. Quéré, Capillarity and Wetting Phenomena: Drops, Bubbles, Pearls, Waves, Springer, New York, 2003.
[25] R.E. Pepper, L. Courbin, H.A. Stone, Splashing on elastic membranes: the importance of early-time dynamics, Phys. Fluids 20 (2008) p. 082103.
[26] P.G. deGennes, Wetting: statics and dynamics, Rev. Mod. Phys. 57 (1985) 827–863.
[27] S.F. Kistler, Hydrodynamics of wetting, in: J.C. Berg (Ed.), Wettability, Dekker, New York, 1993.
[28] Z. Haiman, B. Kocsis, K. Menou, the population of viscosity- and gravitational wave-driven supermassive black hole binaries among luminous active galactic nuclei, Astrophys. J. 700 (2009 Aug) 1952–1969.
[29] J.P. Shelby, J. White, K. Ganesan, P.K. Rathod, D.T. Chiu, A microfluidic model for single-cell capillary obstruction by *Plasmodium falciparum* –infected erythrocytes, Proc. Natl. Acad. Sci. U.S.A. 100 (2003) 14618–14622.
[30] R.H. Naylor, Galileo and the Problem of Free Fall, British Journal for the History of Science 7 (1974) 105–134.
[31] Galileo, Discorsi e dimostrazioni matematiche, intorno à due nuove scienze, translated in 1963 as 'Dialogues concerning two new sciences' by H. Crew and A. de Salvio: Dover, New York, 1638.
[32] S. Taneda, Experimental investigation of the wake behind a sphere at low Reynolds numbers, J. Phys. Soc. Jpn. 11 (1956) 1104–1108.
[33] M. Ozgoren, E. Pinar, B. Sahin, H. Akilli, Comparison of flow structures in the downstream region of a cylinder and sphere, Int. J. Heat Fluid Flow 32 (2011) 1138–1146.
[34] E.J. Lavernia, E.M. Gutierrez, J. Szekely, N.J. Grant, A mathematical model for the liquid dynamic compaction process. Part 1: Heat flow in gas atomization, Int. J. Rapid Solid. 4 (1988) 89–124.
[35] E. Villermaux, Fragmentation, Annu. Rev. Fluid Mech. 39 (2007) 419–446.
[36] L.P. Hsiang, G.M. Faeth, Drop deformation and breakup due to shock-wave and steady disturbances, Int. J. Multiphase Flow 21 (1995 Aug) 545–560.
[37] T.G. Theofanous, Aerobreakup of Newtonian and viscoelastic liquids, in: S.H. Davis P. Moin (Eds.), Annual Review of Fluid Mechanics, vol. 43, Annual Reviews, Palo Alto, 2011, pp. 661–690.
[38] L.I. Sedov, Similarity and Dimensional Methods in Mechanics, tenth edition, CRC Press, 1993.
[39] G.I. Barenblatt, Scaling: Volume 34 of Cambridge Texts in Applied Mathematics, Cambridge University Press, 2003.
[40] R.M. Gardner, Defining the diameter of the smallest parent stain produced by a drip, J. Forensic Identific. 56 (2006) 210–221.
[41] P.A. Pizzola, S. Roth, P.R. De Forest, Blood droplet dynamics. I, J. Forensic Sci. 31 (1986) 36–49.
[42] V. Balthazard, R. Piedelievre, H. Desoille, L. Derobert, Etude des gouttes de sang projete, in: XXIIe congres de medicine legale de langue francaise, Paris, 1939.
[43] U. Buck, B. Kneubuehl, S. Näther, N. Albertini, L. Schmidt, M. Thali, 3D bloodstain pattern analysis: ballistic reconstruction of the trajectories of blood drops and determination of the centres of origin of the bloodstains, Forensic Sci. Int. 206 (2011 Mar 20) 22–28.
[44] A. Armenti (Ed.), The Physics of Sports, American Institute of Physics, 1992.
[45] A. Emes, C. Price, Blood In Slow Motion [a video from the Metropolitain Police Forensic Science Laboratory], 1994.
[46] A.E. Donaldson, N.K. Walker, I.L. Lamont, S.J. Cordiner, M.C. Taylor, Characterising the dynamics of expirated bloodstain pattern formation using high-speed digital video imaging, Int. J. Legal Med. 125 (2011 Nov) 757–762.
[47] J.O. Pex, C.H. Vaughan, Observations of high velocity bloodspatter on adjacent objects, J. Forensic Sci. 32 (1987) 1587–1594.
[48] M.C. Taylor, T.L. Laber, B.P. Epstein, D.S. Zamzow, D.P. Baldwin, The effect of firearm muzzle gases on the backspatter of blood, Int. J. Legal Med. 125 (2011 Sep) 617–628.
[49] T.L. Laber, B.P. Epstein, M.C. Taylor, High speed digital video analysis of bloodstain pattern formation from common bloodletting mechanisms, IABPA News (2008) 4–12.
[50] T.L. Laber, B.P. Epstein, M.C. Taylor, High speed digital video analysis of bloodstain pattern formation from common bloodletting mechanisms, Bloodstain Pattern Analysis Video Collection, Midwest Forensic Center (Ames, IA). Available: www.mfrc.ameslab.gov.
[51] E. MacCurdy, The Notebooks of Leonardo da Vinci, vols. I & II, Reynal and Hitchcock, 1938.
[52] F. Savart, Mémoire sur la constitution des veines liquides lancées par des orifices circulaires en mince paroi, Ann. De Chim. 53 (1833) 337–386.
[53] A.M. Worthington, A second paper on the forms assumed by drops of liquids falling vertically on a horizontal plate, Proc. R. Soc. London 25 (1877) 498–503.
[54] A.M. Worthington, On the forms assumed by drops of liquids falling vertically on a horizontal plate, Proc. R. Soc. London 25 (1876) 261–272.
[55] J.M. Kolinski, S.M. Rubinstein, S. Mandre, M.P. Brenner, D.A. Weitz, L. Mahadevan, Skating on a film of air: drops impacting on a surface, Phys. Rev. Lett. 108 (2012), pp. 074503:1–5.
[56] D. Attinger, Z. Zhao, D. Poulikakos, An experimental study of molten microdroplet surface deposition and solidification: transient behavior and wetting angle dynamics, J. Heat Transfer 122 (2000) 544–556.
[57] A. Velten, E. Lawson, A. Bardagjy, M. Bawendi, R. Raskar, Slow art with a trillion frames per second camera, in: Presented at the ACM SIGGRAPH 2011 Posters, Vancouver, British Columbia, Canada, 2011.

[58] W.D. Bachalo, Experimental methods in multiphase flows, Int. J. Multiphase Flow 20 (1994 Aug) 261–295.
[59] N. Damaschke, H. Nobach, T.I. Nonn, N. Semidetnov, C. Tropea, Multi-dimensional particle sizing techniques, Exp. Fluids 39 (2005) 336–350.
[60] C. Tropea, Optical particle characterization in flows, in: S.H. Davis, P. Moin (Eds.), Annual Review of Fluid Mechanics, vol. 43, Palo Alto, 2011, pp. 399–426 (annual reviews).
[61] S.D.R. Wilson, The slow dripping of a viscous fluid, J. Fluid Mech. 190 (1988 May) 561–570.
[62] J. Eggers, Drop formation – an overview, ZAMM Zeitschrift Angew. Math. Mech. 85 (2005) 400–410.
[63] H.M. Dong, W.W. Carr, J.F. Morris, An experimental study of drop-on-demand drop formation, Phys. Fluids 18 (2006), pp. 072102:1–16.
[64] X.D. Shi, M.P. Brenner, S.R. Nagel, A cascade of structure in a drop falling from a faucet, Science 265 (1994) 219–222.
[65] O.E. Yildirim, O.A. Basaran, Dynamics of formation and dripping of drops of deformation-rate-thinning and -thickening liquids from capillary tubes, J. Non-Newtonian Fluid Mech. 136 (2006 Jun) 17–37.
[66] B. Ambravaneswaran, E.D. Wilkes, O.A. Basaran, Drop formation from a capillary tube: comparison of one-dimensional and two-dimensional analyses and occurrence of satellite drops, Phys. Fluids 14 (2002) 2606–2621.
[67] C. Clanet, J.C. Lasheras, Transition from dripping to jetting, J. Fluid Mech. 383 (1999 Mar) 307–326.
[68] C.D. Stow, M.G. Hadfield, An experimental investigation of fluid flow resulting from the impact of a water drop with an unyielding dry surface, Proc. R. Soc. London A 373 (1981) 419–441.
[69] O.A. Basaran, Nonlinear oscillations of viscous liquid drops, J. Fluid Mech. 241 (1992) 169–198.
[70] D. Attinger, S. Haferl, Z. Zhao, D. Poulikakos, Transport phenomena in the impact of a molten droplet on a surface: macroscopic phenomenology and microscopic considerations. Part II: heat transfer and solidification, Annu. Rev. Heat Transfer XI (2000) 65–143.
[71] A.H. Lefebvre, Atomization and Sprays, Hemisphere, New York, 1989.
[72] I.V. Roisman, K. Horvat, C. Tropea, Spray impact: Rim transverse instability initiating fingering and splash, and description of a secondary spray, Phys. Fluids 18 (2006 Oct).
[73] M. Taylor, Cough through bloodied lips {High Speed Visualization}. Available: https://www.mfrc.ameslab.gov/files/Bloodletting%20Mechanism%20Videos/15Ac3%20Cough%20through%20bloodied%20lips.avi.
[74] D.F. Rutland, G.J. Jameson, A non-linear effect in the capillary instability of liquid jets, J. Fluid Mech. 46 (1971) 267–271.
[75] M.V. Dyke, An Album of Fluid Motion, The Parabolic Press, Stanford California, 1982
[76] E. Villermaux, B. Bossa, Drop fragmentation on impact, J. Fluid Mech. 668 (2011) 412–435.
[77] W.A. Sirignano, C. Mehring, Review of theory of distortion and disintegration of liquid streams, Progr. Energy Combustion Sci. 26 (2000) 609–655.
[78] A. Korobkin, Shallow-water impact problems, J. Eng. Math. 35 (1999 Feb) 233–250.
[79] A.A. Korobkin, Asymptotic theory of liquid–solid impact, Phil. Trans. R. Soc. Lond. A 355 (1997) 507–522.
[80] A.A. Korobkin, V.V. Pukhnachov, Initial stage of water impact, Annu. Rev. Fluid Mech. 20 (1988) 159–185.
[81] S.P. Lin, R.D. Reitz, Drop and spray formation from a liquid jet, Annu. Rev. Fluid Mech. 30 (1998) 85–105.
[82] K. Walcher, Gerichtlich-medizinische und kriminalistische Blutuntersuchung ein Leitfaden fuer Studierende, Aerzte und Kriminalisten; translation of pages 15–33 concerning "The shape of blood stains", Springer, Berlin, 1939 .
[83] P.L. Kirk, Affidavit Regarding State of Ohio V. Samual Sheppard, Court of Common Pleas, Criminal Branch, No. 64571, 26 April 1955.
[84] M.B. Illes, A.L. Carter, P.L. Laturnus, A.B. Yamashita, Use of the BackTrack computer program for bloodstain pattern analysis of stains from downward-moving drops, J. Can. Soc. Forensic Sci. 38 (2005) 213–217.
[85] A.L. Carter, The directional analysis of bloodstain patterns: theory and experimental validation, J. Can. Soc. Forensic Sci. 34 (2001), 173-173.
[86] R. Kanable, BackTrack going forward, Law Enforcement Technol. (2006) 40–45.
[87] A.L. Carter, Validation of the BackTrackTM suite of programs for bloodstain pattern analysis, J. Forensic Identif. 56 (2006) 242–254.
[88] A.L. Carter, M. Illes, K. Maloney, A.B. Yamashita, B. Allen, B. Brown, L. Davidson, G. Ellis, J. Gallant, A. Gradkowski, J. Hignell, S. Jory, P.L. Laturnus, C.C. Moore, R. Pembroke, A. Richard, R. Spenard, C. Stewart, Further validation of the BackTrack(TM) computer program for bloodstain pattern analysis: precision and accuracy, Int. Assoc. Bloodstain Pattern Analysts News 21 (2005) 15–22.
[89] J.K. Wells, Investigation of Factors Affecting the Region of Origin Estimate in Bloodstain Pattern Analysis, MS Thesis, University of Canterbury, 2006.
[90] A.L. Carter, Bloodstain pattern analysis with a computer, in: Scientific and Legal Applications of Bloodstain Pattern Interpretation, CRC Press, Boca Raton, FL, USA, 1998, pp. 17–28.
[91] M. Illes, M. Boué, Investigation of a model for stain selection in bloodstain pattern analysis, Can. Soc. Forensic Sci. J. 44 (2011) 1–12.
[92] M.B. Illes, Investigation of a model for stain selection and a robust estimation for area of origin in bloodstain pattern analysis, MS Thesis, Trent University, Ontario, Canada, 2011.
[93] J. Wells, Investigation of factors affecting the region of origin estimates in bloodstain pattern analysis" [Master's Thesis], University of Canterbury, Canterbury (New Zealand), 2006.
[94] H. Templeman, Errors in blood droplet impact angle reconstruction using a protractor, J. Forensic Identific. 40 (1990) 15–24.
[95] W.F. Rowe, Errors in the determination of the point of origin of bloodstains, Forensic Sci. Int. 161 (2006) 47–51.
[96] C. Connolly, M. Illes, J. Fraser, Affect of impact angle variations on area of origin determination in bloodstain pattern analysis, Forensic Sci. Int. 223 (2012) 233–240.
[97] K.G. de Bruin, R.D. Stoel, J.C.M. Limborgh, Improving the point of origin determination in bloodstain pattern analysis, J. Forensic Sci. 56 (2011) 1476–1482.
[98] P.A. Pizzola, J.M. Buszka, N. Marin, N.D.K. Petraco, P.R. De Forest, Commentary on "3D bloodstain pattern analysis: Ballistic reconstruction of the trajectories of blood drops and determination of the centres of origin of the bloodstains" by Buck et al. [Forensic Sci. Int. 206 (2011) 22–28], Forensic Sci. Int. 220 (2012) e39–e40.
[99] B.T. Cecchetto, Nonlinear Blood Pattern Reconstruction, MS thesis, The University of British Columbia, Vancouver, Canada, 2010.
[100] C.R. Varney, F. Gittes, Locating the source of projectile fluid droplets, Am. J. Phys. 79 (2011) 838–842.
[101] W.D. Flower, The terminal velocity of drops, Proc. Phys. Soc. 40 (1927) 167–176.
[102] D. Denison, A. Porter, M. Mills, R.C. Schroter, Forensic implications of respiratory derived blood spatter distributions, Forensic Sci. Int. 204 (2011 Jan 30) 144–155.
[103] Y. Hardalupas, C.H. Liu, Implications of the Gaussian intensity distribution of laser beams on the performance of the phase Doppler technique, sizing uncertainties, Prog. Energy Combust. Sci. 23 (1997) 41–63.
[104] I. Nagao, K. Matsumoto, H. Tanaka, Characteristics of dimethylsulfide, ozone, aerosols, and cloud condensation nuclei in air masses over the northwestern Pacific Ocean, J. Geophys. Res.-Atmos. 104 (1999) 11675–11693.
[105] J.U. Otaigbe, M.D. Barnes, K. Fukui, B.G. Sumpter, D.W. Noid, bGeneration, characterization, and modeling of polymer micro- and nano-particles, Polym. Phys. Eng. 154 (2001) 1–86.
[106] C. Lacour, D. Durox, S. Ducruix, M. Massot, Interaction of a polydisperse spray with vortices, Exp. Fluids 51 (2011 Aug) 295–311.
[107] L. Hulse-Smith, M. Illes, A blind trial evaluation of a crime scene methodology for deducing impact velocity and droplet size from circular bloodstains, J. Forensic Sci. 52 (2007 Jan) 65–69.
[108] M.A. Raymond, E.R. Smith, J. Liesegang, Oscillating blood droplets – implications for crime scene reconstruction, Sci. Justice – J. Forensic Sci. Soc. 36 (1996) 161–171.
[109] M. Raymond, J. Liesegang, E. Smith, High speed cinematography of blood droplet deformation in flight—implications for crime scene reconstruction—in advances in forensic sciences, in: Proceedings of the 13th Meeting of the International Association of Forensic Sciences, Duesseldorf, Germany, (1993), pp. 200–207.
[110] D.J. Carlson, R.F. Hoglund, Particle drag and heat transfer in rocket nozzles, AIAA J. 2 (1964) 1980–1984.
[111] D. Poulikakos, J. Waldvogel, Heat transfer and fluid dynamics in the process of spray deposition, Adv. Heat Transfer 28 (1996) 1–74.
[112] O.G. Engel, Waterdrop collisions with solid surfaces, J. Res. Nat. Bur. Stand. 54 (1955) 281–298.
[113] M. Pasandideh-Fard, Y.M. Qiao, S. Chandra, J. Mostaghimi, Capillary effects during droplet impact on a solid surface, Phys. Fluids 8 (1996) 650–659.
[114] L. Hulse-Smith, N.Z. Mehdizadeh, S. Chandra, Deducing drop size and impact velocity from circular bloodstains, J. Forensic Sci. 50 (2005) 54–63.
[115] P. Attané, F. Girard, V. Morin, An energy balance approach of the dynamics of drop impact on a solid surface, Phys. Fluids 19 (2007), pp. 012101:1-17.
[116] H.B. Humberstone, Charlie Chan at the race track, 20th Century Fox, 1936.
[117] H. Marmanis, S.T. Thoroddsen, Scaling of the fingering pattern of an impacting drop, Phys. Fluids 8 (1996), 1344-1344.
[118] N.Z. Mehdizadeh, S. Chandra, J. Mostaghimi, Formation of fingers around the edges of a drop hitting a metal plate with high velocity, J. Fluid Mech. 510 (2004 Jul) 353–373.
[119] H.L. MacDonell, L.F. Bialousz, Flight characteristics and stain patterns of human blood, Report to the National Institute of Law Enforcement and Criminal Justice, US Dept of Justice, Law Enforcement Assistance Administration, Washington, DC, 1971.
[120] P.L. Kirk, Crime Investigation: Physical Evidence and the Police Laboratory, Interscience Publishers, 1953.
[121] C. Willis, A.K. Piranian, J.R. Donaggio, R.J. Barnett, W.F. Rowe, Errors in the estimation of the distance of fall and angles of impact blood drops, Forensic Sci. Int. 123 (2001 Nov) 1–4.
[122] C. Rizer, Police Mathematics, Charles C. Thomas, Springfield, IL, 1955, pp. 72–73.
[123] P.A. Pizzola, S. Roth, P.R. De Forest, Blood droplet dynamics. II, J. Forensic Sci. 31 (1986) 50–64.
[124] C. Knock, M. Davison, Predicting the position of the source of blood stains for angled impacts, J. Forensic Sci. 52 (2007) 1044–1049.
[125] J.C. Bird, S.S.H. Tsai, H.A. Stone, Inclined to splash: triggering and inhibiting a splash with tangential velocity, N. J. Phys. 11 (2009), pp. 063017:1–11.
[126] A.L. Yarin, Drop impact dynamics: splashing, spreading, receding, bouncing, Annu. Rev. Fluid Mech. 38 (2005), 159-159.
[127] S. Haferl, Z. Zhao, J. Giannakouros, D. Attinger, D. Poulikakos, Transport phenomena in the Impact of a molten droplet on a surface: macroscopic phenomenology and microscopic considerations. Part I: Fluid dynamics, in: C.L. Tien (Ed.), Annual Review of Heat Transfer, vol. XI, Begell House, NY, 2000, pp. 145–205.
[128] M. Rein, Phenomena of liquid drop impact on solid and liquid surfaces, Fluid Dyn. Res. 12 (1993) 61–93.
[129] F.H. Harlow, J.P. Shannon, The splash of a liquid drop, J. Appl. Phys. 38 (1967) 3855–3866.
[130] M. Bertagnolli, M. Marchese, G. Jacucci, I.S. Doltsinis, S. Noelting, Thermomechanical simulation of the splashing of ceramic droplets on a rigid substrate, J. Comp. Phys. 133 (1997) 205–221.

[131] J. Fukai, Y. Shiba, T. Yamamoto, O. Miyatake, D. Poulikakos, C.M. Megaridis, Z. Zhao, Wetting effects on the spreading of a liquid droplet colliding with a flat surface: experiment and modeling, Phys. Fluids 7 (1995) 236–247.
[132] Z. Zhao, D. Poulikakos, J. Fukai, Heat transfer and fluid dynamics during the collision of a liquid droplet on a substrate: II—experiments, Int. J. Heat Mass Transfer 39 (1996) 2791–2802.
[133] T.D. Blake, J. DeConinck, The influence of solid–liquid interactions on dynamic wetting, Adv. Colloid Interface Sci. 66 (2002) p. 21.
[134] R. Bhardwaj, D. Attinger, Non-isothermal wetting during impact of millimeter size water drop on a flat substrate: numerical investigation and comparison with high speed visualization experiments, Int. J. Heat Fluid Flow 29 (2008) 1422–1435.
[135] D. Attinger, D. Poulikakos, Melting and resolidification of a substrate caused by molten microdroplet impact, J. Heat Transfer 123 (2001) 1110–1122.
[136] C. Mundo, M. Sommerfeld, C. Tropea, Droplet-wall collisions: experimental studies of the deformation and breakup process, Int. J. Multiphase Flow 21 (1995) 151–173.
[137] R. Rioboo, C. Bauthier, J. Conti, M. Voué, J. De Coninck, Experimental investigation of splash and crown formation during single drop impact on wetted surfaces, Exp. Fluids 35 (2003) 648–652.
[138] P. Roura, J. Fort, Comment on effects of the surface roughness on sliding angles of water droplets on superhydrophobic surfaces, Langmuir 18 (2002) 566–569.
[139] T. Mao, D.C.S. Kuhn, H. Tran, Spread and rebound of liquid droplets upon impact on flat surfaces, AIChE J. 43 (1997) 2169–2179.
[140] S. Chandra, C.T. Avedisian, On the collision of a droplet with a solid surface, Proc. R. Soc. Lond. A 432 (1991) 13–41.
[141] C. Josserand, L. Lemoyne, R. Troeger, S. Zaleski, Droplet impact on a dry surface: triggering the splash with a small obstacle, J. Fluid Mech. 524 (2005) 47–56.
[142] S. Mandre, M.P. Brenner, The mechanism of a splash on a dry solid surface, J. Fluid Mech. 690 (2012) 148–172.
[143] L. Xu, W.W. Zhang, S.R. Nagel, Drop splashing on a dry smooth surface, Phys. Rev. Lett. 94 (2005), pp. 184505:1–4.
[144] R.E. Ford, C.G.L. Furmidge, Impact and spreading of spray drops on foliar surfaces, Wetting 25 (1967) 417–432.
[145] M.B. Lesser, Analytic solutions of liquid-drop impact problems, Proc. Roy. Soc. London A 377 (1981) 289–308.
[146] J.E. Field, J.P. Dear, J.E. Ogren, The effects of target compliance on liquid drop impact, J. Appl. Phys. 62 (1988) 533–540.
[147] A. Joshi, Y. Sun, Wetting dynamics and particle deposition for an evaporating colloidal drop: a lattice Boltzmann study, Phys. Rev. E 82 (2010).
[148] I.S. Bayer, C.M. Megaridis, Contact angle dynamics in droplets impacting on flat surfaces with different wetting characteristics, J. Fluid Mech. 558 (2006 Jul 10) 415–449.
[149] Š. Šikalo, C. Tropea, E.N. Ganic, Dynamic wetting angle of a spreading droplet, Exp. Therm. Fluid Sci. 29 (2005) 795–802.
[150] D. Attinger, An Investigation of Molten Microdroplet Surface Deposition: Transient Behavior, Wetting Angle Dynamics and Substrate Melting Phenomenon; Ph.D. thesis, Department of Mechanical Engineering, Eidgenoessische Technische Hochschule (ETH), Zurich, 2001.
[151] L. Chen, Z. Li, Bouncing droplets on nonsuperhydrophobic surfaces, Phys. Rev. E 82 (2010).
[152] D. Caviezel, C. Narayanan, D. Lakehal, Adherence and bouncing of liquid droplets impacting on dry surfaces, Microfluid. Nanofluid. 5 (Oct 2008) 469–478.
[153] D. Bartolo, F. Bouamrirene, E. Verneuil, A. Buguin, P. Silberzan, S. Moulinet, Bouncing or sticky droplets: impalement transitions on superhydrophobic micropatterned surfaces, Europhys. Lett. 74 (2006) 299–305.
[154] C.G.L. Furmidge, Studies at phase interfaces. I. The sliding of liquid drops on solid surfaces and a theory for spray retention, J. Colloid Sci. 17 (1962) 309–324.
[155] R.D. Deegan, O. Bakajin, T.F. Dupont, G. Huber, S.R. Nagel, T.A. Witten, Capillary flow as the cause of ring stains from dried liquid drops, Nature 389 (1997) 827–829.
[156] D. Brutin, B. Sobac, B. Loquet, J. Sampol, Pattern formation in drying drops of blood, J. Fluid Mech. 667 (2011) 85–95.
[157] R.E. Brown, R.I. Hawkes, M.A. Parker, J.H. Byrd, Entomological Alteration of Bloodstain Evidence, in: Entomological Alteration of Bloodstain Evidence: The Utility of Arthropods in Legal Investigations, CRC Press, Boca Raton, FL, 2001, pp. 353–378.
[158] A. Becue, S. Moret, C. Champod, P. Margot, Use of quantum dots in aqueous solution to detect blood fingermarks on non-porous surfaces, Forensic Sci. Int. 191 (2009 Oct 30) 36–41.
[159] S. Boyd, M.F. Bertino, S.J. Seashols, Raman spectroscopy of blood samples for forensic applications, Forensic Sci. Int. 208 (2011) 124–128.
[160] R.H. Bremmer, K.G. de Bruin, M.J. van Gemert, T.G. van Leeuwen, M.C. Aalders, Forensic quest for age determination of bloodstains, Forensic Sci. Int. 216 (2012) 1–11.
[161] D. Brutin, B. Sobac, C. Nicloux, Influence of substrate nature on the evaporation of a sessile drop of blood, J. Heat Transfer-Trans. ASME 134 (2012 Jun).
[162] M. Kaibara, Rheology of blood coagulation, Biorheology 33 (1996) 101–117.
[163] W.D. Ristenpart, P.G. Kim, C. Domingues, J. Wan, H.A. Stone, Influence of substrate conductivity on circulation reversal in evaporating drops, Phys. Rev. Lett. 99 (2007), pp. 234502:1–4.
[164] R. Bhardwaj, X. Fang, P. Somasundaran, D. Attinger, Self-assembly of colloidal particles from evaporating droplets: role of the pH and proposition of a phase diagram, Langmuir 26 (2010) 7833–7842.
[165] H. Hu, R.G. Larson, Evaporation of a sessile droplet on a substrate, J. Phys. Chem. B 106 (2002) 1334–1344.
[166] H. Hu, R.G. Larson, Analysis of microfluid flow in an evaporating sessile droplet, Langmuir 21 (2005) 3963–3971.
[167] B.J. Fischer, Particle convection in an evaporating droplet, Langmuir 18 (2002) 60–67.
[168] H. Hu, R.G. Larson, Marangoni effect reversed coffee-ring depositions, J. Phys. Chem. B 110 (2006) 7090–7094.
[169] E. Widjaja, M.T. Harris, Particle deposition study during sessile drop evaporation, AIChE J. 54 (2008) 2250–2260.
[170] R. Bhardwaj, X. Fang, D. Attinger, Pattern formation during the evaporation of a colloidal nanoliter drop: a numerical and experimental study, N. J. Phys. 11 (2009), pp. 075020:1–33.
[171] E.W. Washburn, The dynamics of capillary flow, Phys. Rev. 17 (1921) 273–283.
[172] J. Xiao, H.A. Stone, D. Attinger, Source-like solution for radial imbibition into a homogeneous semi-infinite porous medium, Langmuir 28 (2012) 4208–4212.
[173] B. Simoncic, V. Rozman, Wettability of cotton fabric by aqueous solutions of surfactants with different structures, Colloids Surf. A: Physicochem. Eng. Aspects 292 (2007) 236–245.
[174] C. Allain, L. Limat, Regular patterns of cracks formed by directional drying of a colloidal suspension, Phys. Rev. Lett. 74 (1995) 2981–2984.
[175] N. Robinson, L. Schattenberg, M. Zorzoli, P. Mangin, M. Saugy, Haematological analysis conducted at the departure of the Tour de France 2001, Int. J. Sports Med. 26 (2005) 200–207.
[176] J.S. Mørkeberg, B. Belhage, R. Damsgaard, Changes in blood values in elite cyclist, Int. J. Sports Med. 30 (2009) 130–138.
[177] R. Bhardwaj, J.P. Longtin, D. Attinger, Interfacial temperature measurements, high-speed visualization and finite-element simulations of droplet impact and evaporation on a solid surface, Int. J. Heat Mass Transfer 53 (2010) 3733–3744.
[178] T.D. Blake, R.A. Dobson, K.J. Ruschak, Wetting at high capillary numbers, J. Colloid Interface Sci. 279 (2004 Nov 1) 198–205.
[179] S.R. Ranabothu, C. Karnezis, L.L. Dai, Dynamic wetting: hydrodynamic or molecular-kinetic? J. Colloid Interface Sci. 288 (2005) 213–221.
[180] J.B. Freund, The atomic detail of a wetting/de-wetting flow, Phys. Fluids 15 (2003) L33–L36.
[181] H.L. MacDonell, Age of a bloodstain before it was wiped, CD describing research work of F. Trassati, in: Meeting with D. Attinger, January 2010.
[182] S. Sikalo, E.N. Ganič, Phenomena of droplet–surface interactions, Exp. Therm. Fluid Sci. 31 (2006) 97–110.
[183] M. Pasandideh-Fard, S. Chandra, J. Mostaghimi, A three-dimensional model of droplet impact and solidification, Int. J. Heat Mass Transfer 45 (2002) 2229–2242.
[184] R. Rioboo, M. Marengo, C. Tropea, Time evolution of liquid drop impact onto solid, dry surfaces, Exp. Fluids 33 (2002) 112–124.
[185] M. Miwa, A. Nakajima, A. Fujishima, K. Hashimoto, T. Watanabe, Effects of the surface roughness on sliding angles of water droplets on superhydrophobic surfaces, Langmuir 16 (2000) 5754–5760.
[186] B.F. Gelfand, Droplet breakup phenomena in flows with velocity lag, Prog. Energy Combust. Sci. 22 (1996) 201–265.
[187] L. Cheng, Dynamic spreading of drops impacting onto a solid surface, Ind. Eng. Chem. 16 (1977) 192–197.
[188] C. Corby, C. Hauke, B. Gestring, L. Quarino, Preliminary study analyzing the halo effect: factors involved in sequencing the deposition of overlapping bloodstains caused by wipe patterns and blood droplets, Investig. Sci. J. 4 (2012).
[189] F. Chafe, Determination of impact angle using mathematical properties of the ellipse, Int. Assoc. Bloodstain Pattern Analysts News 19 (2003) 5–9.
[190] H.L. MacDonell, No more strings, no more computers, just simple mathematics, that's all it takes, International Association of Bloodstain Pattern Analysts News 12 (1996), 10-10.
[191] B.G. Stephens, T.B. Allen, Back spatter of blood from gunshot wounds. Observations and experimental simulation, J. Forensic Sci. 28 (1983) 437–439.
[192] H. Fujimoto, Y. Shiotani, A. Tong, T. Hama, H. Takuda, Three-dimensional numerical analysis of the deformation behavior of droplets impinging onto a solid substrate, Int. J. Multiphase Flow 33 (2007) 317–332.
[193] K.V. Beard, H.R. Pruppacher, A determination of the terminal velocity and drag of small water drops by means of a wind tunnel, J. Atmos. Sci. 26 (1969) 1066–1072.
[194] S.T. Thoroddsen, J. Sakakibara, Evolution of the fingering pattern of an impacting drop, Phys. Fluids 10 (1998) 1359–1374.
[195] A.L. Gonor, V.Y. Yakovlev, Dynamics of the impact of a drop on a solid surface, Fluid Dyn. 13 (1978) 25–31.
[196] R. Bhardwaj, X. Fang, P. Somasundaran, D. Attinger, Self-assembly of colloidal particles from evaporating droplets: role of DLVO interactions and proposition of a phase diagram, Langmuir 26 (2010) 7833–7842.
[197] G. Berteloot, C.T. Pham, A. Daerr, F. Lequeux, L. Limat, Evaporation-induced flow near a contact line: Consequences on coating and contact angle, EPL (Europhys. Lett.) 83 (2008), pp. 14003:1–5.
[198] Y. Pomeau, E. Villermaux, Two hundred years of capillarity research, Phys. Today 59 (2006) 39–44.
[199] C.M. Reed, N. Wilson, The fundamentals of absorbency of fibres, textile structures and polymers. I. The rate of rise of a liquid in glass capillaries, J. Phys. D: Appl. Phys. 26 (1993) 1378.
[200] E.M.F. D'Albe, M.S. Hidayetulla, The break-up of large water drops falling at terminal velocity in free air, Q. J. R. Meteorol. Soc. 81 (1955) 610–613.
[201] B. Simončič, V. Rozman, Wettability of cotton fabric by aqueous solutions of surfactants with different structures, Colloids Surf. A: Physicochem. Eng. Aspects 292 (2007) 236–245.